

CHAPTER 4: SYNTHESIS AND CHARACTERIZATION OF Au-CONTAINING Me-MCM-41 (Me = Si, Co, Fe)

4.1. Introduction

Amongst the PGMs, gold has a long-standing historic reputation as a catalytically inert metal [1, 2]. However, it was demonstrated in the late 1980s that Au could be used as a catalyst [3, 4] if it is prepared in the form of highly dispersed nanoparticles on metal oxide supports. Since then, the catalytic importance of supported gold nanoparticles has been realized in a number of industrially and environmentally important reactions [5], including CO oxidation [4, 6-9], reduction of nitrogen oxides [10], and the epoxidation of propylene [11-13]. What makes gold catalysts remarkable in the catalyzed reactions is the low temperature at which the catalysis is effected. The CO oxidation reaction (and the selective CO oxidation in the presence of hydrogen) has been widely investigated, and has led to the realization of the key requirements for the exceptionally high activity of gold-based catalysts [8, 14]. These requirements include, among others, the small particle size, the use of “reactive” supports, and a preparation method that achieves the required size of particles in intimate contact with the support. The unexpected behaviour of gold nanoparticles (i.e., their reactivity toward adsorption of O₂ and CO) has been attributed to factors such as the quantum-size effect when the Au particle diameters are in the range 2-5 nm, and the electronic interaction of metal nanoparticles with the oxide support [11, 15].

Figure 4.1 below shows an example of the dependence of CO oxidation activity on the Au particle size [16]:

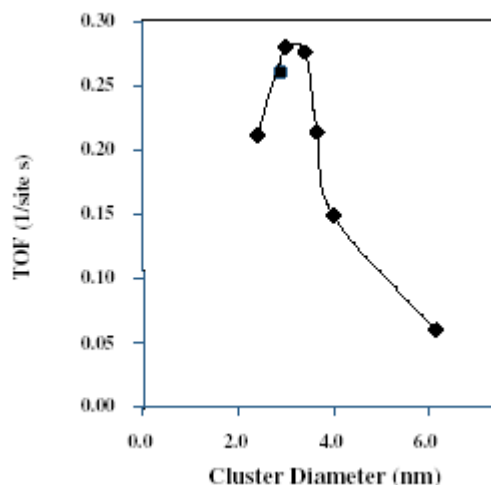


Figure 4.1. Variation of CO oxidation activity as a function of Au cluster size for the model Au/TiO₂(001)/Mo(100) system [16].

As seen, the highest catalytic activity is obtained when the diameter of Au nanoparticles is ~3 nm.

This breakthrough discovery of the loss of “nobleness” at nanometric sizes has since diversified the applications of gold nanoparticles into fields other than catalysis. These include the application of gold nanoparticles in various materials, such as analytical probes [17, 18], microelectronics [19, 20], biological markers [21, 22], colourings [23], sensors [24, 25] and nonlinear optic materials [26].

All these versatile applications are mainly based on the interesting physicochemical properties arising from the size effects of the gold nanoparticles. Therefore, there is a growing need to develop a simple method for preparing these remarkable nanosized metal particles. A number of synthetic techniques have been reported to achieve this purpose during the last decade.

To place the work in this chapter in perspective, a review of the synthetic strategies used that relate to the synthesis of oxidative catalysts (and in particular CO oxidation and propylene epoxidation) will be reviewed.

4.1.1 Synthesis of Supported Gold Nanoparticles: General

Supported gold catalysts, with a high degree of dispersion and with particle sizes below 5 nm, are known to be highly active for CO oxidation at low temperature. Different synthesis methods [27-29] and different support types [27, 30-32] lead to different properties of the resulting catalyst systems. Another variable associated with the synthesis of active Au catalysts for the CO oxidation reaction is the method of *pretreatment* of the catalyst precursor [33-36]. Since the nature of the support is one of the factors influencing the exceptional activity of supported Au catalysts, particularly the CO oxidation reaction, the synthesis of supported Au catalysts using different supports will be briefly reviewed in the next sections. Different synthetic approaches are required to produce the different supports in order to prepare highly dispersed and active Au catalysts. Different supports vary in properties such as the point of zero charge and the extent of interaction with the catalytic species.

4.1.2. Gold Nanoparticles on Haruta-type Supports

Because of the lower melting point of gold compared to that of other platinum group metals (Au = 1336 K, Pd = 1823 K and Pt = 2042 K), and the fact that gold in a highly dispersed state has a much lower melting point (~600 K) due to the quantum size effect [37], it is difficult to prepare highly dispersed gold catalysts by the conventional wet-impregnation methods. However, other synthesis methods such as deposition-precipitation (DP) [38, 39], coprecipitation (CP) [6] and vapour deposition (VD) [40, 41] can be successfully employed to obtain highly dispersed nano-gold catalysts. DP has the advantage over CP in that it yields a narrow particle size distribution and has Au localized only on the surface of the support [42]. On supports like

SiO₂, vapour deposition techniques like chemical vapour deposition (CVD) and physical vapour deposition (PVD) [16, 40] are preferred to liquid-phase methods such as DP and CP.

Recent advances in the search for preparative methods have led to an approach involving the grafting of gold-phosphine complexes on the support [27, 35], and a detailed review of this procedure has been published by Kozlov et al [43]. On the basis of the support-dependence of Au catalytic activity, the oxidic supports have been divided into two main classes [32]: active supports (reducible metal-oxides) and inert supports (e.g. SiO₂, Al₂O₃, etc).

Even though CP is a common method for producing highly active supported gold catalysts, other preparation methods are being evaluated in order to find simple preparation methods for the low temperature Au-catalyzed CO oxidation reaction. It seems likely that a metal-support interaction, which is stronger when gold is coprecipitated together with the metal oxide support, is responsible for the enhanced catalytic activity in CO oxidation reaction. Strong metal-support interactions (SMSIs) yields high metal dispersions and thus a high density of catalytic sites, while catalysts with weak metal-support interactions lead to aggregation of the metal species [44, 45].

The preparation of highly active gold catalysts has been reported in which both (i) deposition-precipitation of aqueous solutions of HAuCl₄ with Na₂CO₃ or NH₄OH at pH 6-10 on oxide supports and (ii) chemical vapour deposition of organometallic gold precursors onto oxide supports has been achieved [5, 8]. Through the interaction of anionic Au(III) precursors with a positively charged oxide surface, active TiO₂, Fe₂O₃ and Al₂O₃ supported gold catalysts have been prepared. Their catalytic activities were found to be strongly dependent on the preparation and pretreatment conditions [15]. Direct impregnation of AuCl₃ or HAuCl₄ on calcined silicas to produce supported gold catalysts was considered to be complicated due to lack of exchange (or lack of adsorption sites for anionic metal precursors) on the negatively charged

surface. Furthermore, a high pH condition causes the dissolution of the SiO₂ support [15, 46]. Homogeneous deposition-precipitation (HDP) using urea as a precipitating agent has been used to prepare Al₂O₃-supported Au catalysts [47].

In spite of the success with some inert supports, the preparation of active Au/SiO₂ catalysts using solution-based methods is difficult to achieve, and the resulting materials have very low activity in CO oxidation [15, 48]. In the case of SiO₂, the DP technique fails to produce active CO oxidation catalysts, because the low isoelectric point of SiO₂ (between 1 and 2), renders the surface charge highly negative at the synthesis pH used. However, functionalizing the mesoporous SiO₂ surface with cationic organosilanes to generate a monolayer of positively charged groups on the pore surface affords active silica-supported gold nanoparticles [49], i.e. the DP method was found to be an unsuitable procedure to produce Au/SiO₂ materials.

The importance of the preparation method for CO oxidation catalysts has been clearly demonstrated by Bamwenda et al [29], who observed orders of magnitude higher activity in catalysts prepared by deposition-precipitation compared to catalysts prepared by photodeposition and impregnation methods. There seems to be a general consensus in the literature that the coprecipitation (CP) and deposition-precipitation (DP) preparative routes lead to highly dispersed and active catalysts for the CO oxidation reaction. The operational procedures for these two methods are outlined below.

(i) Coprecipitation (CP)

In this method, an aqueous solution containing both HAuCl₄ and a metal nitrate (i.e., the support precursor) is added to an aqueous solution of Na₂CO₃ to produce a hydroxide or carbonate precipitate, i.e. the support and metal are precipitated simultaneously. After further stirring and aging, the coprecipitate is washed free of the Cl⁻

ions, dried and finally calcined in air at a temperature above 250 °C to produce Au particles smaller than 10 nm.

A variant of this method, termed “inverse coprecipitation” by Wagner et al [50] involves addition of an aqueous solution of Na₂CO₃ (7.5 ml/min) into an aqueous mixture of HAuCl₄ and Fe(NO₃)₃·9H₂O at 75 °C under vigorous (500 rpm) stirring. The resulting coprecipitate is kept stirring in the mother liquor at 75 °C for 8 - 20 h before being washed for several hours with hot water until free of the chloride ions.

(ii) Deposition-precipitation (DP)

After the pH of an aqueous solution of HAuCl₄ is adjusted to a fixed point in the range 6-10, a pre-formed metal oxide support (powder, bead, honeycomb, or thin film) is immersed in the solution. Aging for about 1 hour results in the deposition of Au(OH)₃ exclusively on the surface of metal oxide support once the concentration and temperature are properly chosen. After product recovery by filtration, it is washed several times with distilled or deionized water to remove Cl⁻ ions, dried and calcined to obtain the final catalyst. This often produces gold nanoparticles in the 4-6 nm size range.

4.1.3 Gold Nanoparticles on Conventional Zeolite Supports

Zeolites have been used as supports for loading Au nanoparticles, and a range of methods have been developed to prepare Au/Y-type zeolite catalysts: (i) Au₂Cl₆ was used by Ichikawa to prepare Au(I)/NaY via a solid-vapour reaction [51-53], (ii) Fraissard and coworkers [54, 55] used [Au(en)₂]Cl₃ to prepare Au/NaY via a cation exchange process, (iii) Kang and Wan [56-58] prepared gold in a Y-type zeolite from a chloroauric acid solution (HAuCl₄·3H₂O) by ion exchange and (iv) Salama et al [59] prepared homogeneously dispersed Au(I)/Na-Y nanoparticles by mechanically mixing Au₂Cl₆ and the zeolite at room temperature under a N₂ atmosphere.

Gao et al [60] have also reported the synthesis of Au/MFI materials by sublimation of AuCl₃ onto MFI. The sublimation method has also been used to prepare Au/zeolite-A by interacting AuCl₃ with zeolite-A in a closed ampoule [61]. Gold has also been loaded into FSM-16 and Y zeolites by mechanical mixing under a nitrogen atmosphere [62]. This physical mixing method was also used to prepare other Au/Zeolite (Zeolite = NaY, Na-mordenite, and Na-ZSM-5) catalysts from AuCl₃ [63], while others have reported the preparation of Au/ZSM-5 by direct hydrothermal synthesis [64].

Au-Fe/HY zeolites containing highly stable Au nanoparticles inside the zeolite supercages have been prepared by co-exchange of Fe(II)ethylenediammonium and Au(III)-ethylenediamine complex ions into HY zeolite [65].

4.1.4 Gold Nanoparticles on Mesoporous Zeolite Supports

Mesoporous silica materials (MCM-41, MCM-48 and SBA-15) are suitable host materials for Au nanoparticles because of their attractive properties that include: ordered channel structure, a narrow pore size distribution (diameters in the range 1.5 – 10 nm) and large specific surface areas ($\geq 1000 \text{ m}^2/\text{g}$, see Chapters 1 and 2).

In mesoporous nanocomposite materials, Au/MCM-41 has been synthesized [66] by stabilizing Au nanoparticles via an organic functionality on the surface of MCM-41. Recently, Liu et al [67] have synthesized Au nanoparticles confined in mesoporous aluminosilicate MCM-41 by a direct one-pot synthesis. The size effect on the catalytic activity was also demonstrated in this work. A gold catalyst containing 24 wt% Au on SiO₂ showed the highest CO conversion (70 %). Chao et al [68] have prepared highly dispersed Au nanoparticles in mesoporous silica SBA-15 by the silanation of the interchannel surface with (CH₃O)₃Si(CH₂)₃N(CH₃)₃Cl to generate ion-exchange sites for attachment of Au(OH)_nCl_{4-n}⁻ (n = 0 - 4) to produce uniformly dispersed gold nanoparticles in the host channels after further reduction. Importantly,

the average particle size of the metal nanoparticles was found to depend on the pH value of the gold precursor solution. The DP method has been successfully used to prepare Au catalysts on micelle-templated mesoporous Ti materials (Ti-MCM-41 and Ti-MCM-48) [12, 69, 70]. The resulting materials are active for propene epoxidation.

In another synthesis approach, preformed gold nanoparticles of 2 and 5 nm diameter were added to a silica source and an organic template mixture, resulting in the encapsulation of Au in the mesoporous silica structure (SBA-15 and MCM-41 or MCM-48) [71]. In yet another case, gold nanoparticles were formed by in situ reduction of aqueous chloraurate ions mixed with amine- or thiol-modified MCM-41 [72, 73] or with bifunctional amine silane complexes in an MCM-41 precursor solution [74]. In these methods, the removal of template molecules at low temperature is usually required to avoid the aggregation of gold nanoparticles. A novel approach was recently demonstrated [75] that entailed functionalizing the template-free silica with positively charged groups, to make the surface adsorb anionic Au complexes. The adsorbed AuCl_4^- was then reduced by H_2 or NaBH_4 treatment to produce active Au species for the CO to CO_2 oxidation reaction. Gold nanoparticles have also been prepared in amine-functionalized MCM-41 organic-inorganic hybrid materials [76].

4.1.5 Characterization of Supported Gold Nanoparticles

The recognition of the potential of supported Au catalysts has led to the development and use of a number of physicochemical characterization techniques to gain insight into the nature of the gold species produced. Some of the many techniques used are listed in Table 4.1.

Table 4.1. Representative characterization techniques for supported Au catalysts

Catalyst	Characterization techniques	Reference(s)
Au/ γ -Al ₂ O ₃	XRD, TEM, Mossbauer spectroscopy	77
Au/metal oxide	XRD, BET, TEM, ICP, XRF, XPS	6
Au/SBA-15	XRD, TEM, TGA, N ₂ porosimetry, EXAFS, XANES	68
Au/Ti-MCM-41 and -48	TEM, ICP, XPS	69
Au(I)/NaY zeolite	XRD, EXAFS/XANES, UV-Vis spectroscopy	59
Au/MCM-41	XRD, UV-Vis spectroscopy, TEM, XPS, EDX and N ₂ adsorption	66
Au/Zeolite A	DRS UV-Vis spectroscopy, XRD	61
Au/ZSM-5	XRD, ICP, UV-Vis, XPS, N ₂ adsorption/desorption	64
Au/ "active" supports	XRD, AAS, TEM	32
Au/as-synthesized M(OH) _x	XRD, TEM, EXAFS, N ₂ adsorption	35
Au/Al(OH) ₃ or Au/Zn(OH) ₂	XRD, SEM, HRSEM, EDS, TEM, BET, DTA/TGA, Mössbauer spectroscopy	78
Au/spr-Al ₂ O ₃ ; Au/TiO ₂	XRD, BET, XPS, EXAFS, XANES	79, 80
Au/TiO ₂	TEM, XPS, DRIFTS	81
Au/ γ -Al ₂ O ₃ ; Au/MO _x /Al ₂ O ₃	XRD, HRTEM, EDX, AAS	47
Au/ γ -Al ₂ O ₃	EXAFS	82

Comparison of the techniques applied to the different gold supported catalysts reveals the common procedures used: XRD, electron microscopies and N₂ adsorption-

desorption analysis. These techniques have also been used to characterize the materials prepared in this chapter.

4.1.6 Aim of Study

In this work, the high surface area MCM-41 has been chosen as a support for Au. This material is highly porous and has a high S_{BET} area that can help to reduce the amount of precious metal needed to attain high activity. In this chapter we have explored the synthesis of mono- and bimetallic Au/Me-MCM-41 nanocomposite materials (Me = Si, Fe and Co). The aim of introducing the second metal was threefold: (1) to increase the Au-support interactions, which are weak on pure silica MCM-41, (2) to provide nucleation/anchoring sites for the Au nanoparticles, and (3) to induce reducibility properties in the support (Si-MCM-41). Different preparation methods were undertaken to synthesize Au-containing Me-MCM-41 materials having different amounts of Au and Co or Fe in the final samples. The use of these materials as catalysts in the CO oxidation reaction will be discussed in the next chapter.

The synthetic methods used in this chapter can be divided into three broad classes:

- (i) Sol-gel synthesis involving a surfactant (CTAB) templating route to prepare mesoporous metal-silica nanocomposite materials.
- (ii) A deposition-precipitation type of synthesis in which aqueous Au(III) was precipitated in the presence of preformed Me-MCM-41 (Me = Si, Co and Fe).
- (iii) Coprecipitation of aqueous solutions containing ($\text{Au}^{3+}/\text{Me}^{3+/2+}$) ions with sodium carbonate in the presence of preformed calcined Si-MCM-41 ($\text{Me}^{3+} = \text{Fe}^{3+}$ and $\text{Me}^{2+} = \text{Co}^{2+}$).

4.2. Experimental

4.2.1. Materials

For the preparation of the support materials, Si-MCM-41, Fe-MCM-41 and Co-MCM-41, the following chemicals were used: Sodium silicate (Fischer Scientific, 9.1 % Na₂O, 29.2 % SiO₂, 61.7 % H₂O), Cetyltrimethylammonium bromide (CTAB) (Aldrich, 98 %), Fe(NO₃)₃·9H₂O (J. T. Baker, 100.2 %), Co(NO₃)₂·6H₂O (Aldrich, 98 %), 1 M ethylenediamine (en) solution, 2 M Na₂CO₃ or 2 M NaOH solution, 1 M HNO₃ solution and distilled water. In some cases, TEOS (Aldrich) was used as a silica source. For the Au precursor, HAuCl₄·H₂O (Aldrich, 99.999 %) was used. All chemicals were used as obtained from the suppliers, without any further purification.

4.2.2. Synthesis of Mesoporous Au/Me-MCM-41 (Me = Si, Co, Fe)

The synthesis of Si-MCM-41 was given in chapter 2, while that of both Fe- and Co-MCM-41 was reported in chapter 3. Except in the case of the template-directed synthesis of gold-MCM-41 nanocomposites (calcined at 500 °C for 12 h to remove the surfactant), all samples were calcined at 400 °C unless stated otherwise.

The exact metal content of the final materials was not determined. All the compositions given in this study are nominal compositions, calculated on the basis of the initial gel contents. The percentages are calculated relative to SiO₂ assuming that (i) silicate condensation is complete, (ii) all the CTAB template is completely burnt off, and (iii) there is no loss of the metal during calcination.

4.2.2.1 One-Pot Synthesis of Au-containing MCM-41: Direct 80-100 °C Synthesis

In this method, the Au precursor solution was introduced into the Si-MCM-41 precursor gel prior to hydrothermal synthesis in order to obtain Au/MCM-41. The Co- or Fe-containing Au derivatives were prepared by mixing Au(III) with either Fe(III) or Co(II) in water and then adding the solution to the surfactant solution followed by water-glass addition. In some experiments, the synthesis temperature was kept as low as 80 °C for 6 h. The resulting materials were then calcined at 500 °C for 12 h.

In one synthesis, both Fe(III) and Au(III) were both coprecipitated from their aqueous solution using water-glass, which was used both as precipitant and SiO₂ source. After homogenizing this synthesis mixture by magnetic stirring, hydrothermal synthesis was carried out at 100 °C for 5 days. The resulting material was divided into two portions, which were subsequently calcined at 450 °C and 560 °C, respectively. The nominal composition of this material was 1.92 wt% Au/6.5 wt% Fe-MCM-41.

4.2.2.2 Post-Synthesis Approach to Au-containing MCM-41: Ethylenediamine route

This approach is an analogue of the deposition-precipitation method. An Au precursor solution was equilibrated under magnetic stirring with calcined Si-MCM-41 for 1 hour. Then 1M ethylenediamine solution was added dropwise to the stirred suspension, followed by stirring at ambient temperature for 13 h. AuCl₄⁻ was also introduced into calcined Fe- or Co-MCM-41 materials by a similar procedure. After recovering the solid product by filtration and repeatedly washing the mesoporous derivative with warm water to remove the Cl⁻ ions, the material was dried under suction at room temperature and calcined at 400 °C for 4 h unless otherwise stated.

4.2.2.3 Post-Synthesis Approach to Au-containing MCM-41: Coprecipitation route

This synthetic method involved the coprecipitation of the Au(III)-Fe(III) or Au(III)-Co(II) aqueous solutions in the presence of the preformed and calcined Si-MCM-41. Calculated amounts of ferric nitrate nonahydrate or cobaltous nitrate hexahydrate were dissolved into an appropriate volume of a 0.01515 M solution of Au(III) to which 10 ml of distilled water had been added, and the mixture was homogenized with magnetic stirring. This was followed by the slow addition of the siliceous MCM-41 and the suspension was stirred for 15 minutes. A solution of 2 M Na₂CO₃ was then added to the stirred suspension to co-precipitate the metal ions and to increase the final pH to ~9. Stirring was continued for the next 1 h. The suspension was then aged overnight at room temperature, filtered off and the solid washed free of Cl⁻ ions. The resulting samples were either air-dried or briefly oven-dried, without calcination.

4.2.2.4 Post-Synthesis Approach to Au-containing MCM-41: Miscellaneous

A number of other synthesis procedures were attempted: (i) homogeneous precipitation of Au(III) with urea at 90 °C in the presence or preformed Fe-MCM-41 obtained through direct hydrothermal synthesis, (ii) citrate reduction of the Au(III) solution in the presence of preformed Fe-MCM-41, (iii) incipient wetness impregnation of the Au/Fe-MCM-41 material prepared via the ethylenediamine route, and (iv) use of an as-synthesized (uncalcined) Si-MCM-41 material to interact with the AuCl₄⁻ prior to treatment with the ethylenediamine.

4.2.3. Characterization of Au/Me-MCM-41 (Me = Si, Fe, Co)

The new gold-containing materials were characterized by XRD, BET surface area measurement, HRTEM and EDS (see chapters 2 and 3).

The EDS spectra of 5 wt% Au/14 wt% Fe-MCM-41 and 2.28 wt% Au/CTAB-Si-MCM-41 are included in *appendix A.5*, and they confirm the presence of Si, Fe, Au and Si, Au, respectively.

4.3. Results and Discussion

4.3.1 X-ray Diffraction Studies

Direct hydrothermal synthesis of a Au-Fe/MCM-41 bimetallic material was carried out at 100 °C for 5 days by initially coprecipitating the Au(III) and Fe(III) from an aqueous solution using water-glass as a precipitant, followed by addition of the other synthesis gel components. After calcination of the resulting material at two different temperatures (450 and 560 °C), the materials showed structural features illustrated by the XRD patterns in Figure 4.2 (*see below*). This figure shows that the resulting materials are still mesoporous, with reduced long-range order implied by the existence of less-resolved higher order peaks in the low-angle region of the spectrum. By analogy with literature reports [83 - 85], the prominent two peaks appearing in the metal oxide region at about 38 and 44.6° 2 θ are characteristic of FCC Au nanoparticles. The apparently small Fe-related diffraction peaks in the above patterns may suggest the involvement of Fe in the framework of the silicate, while the broad bands between 20 and 30° 2 θ confirm the presence of an amorphous silica phase in these materials. The reduction behaviour of the sample calcined at 560 °C for 6 h was shown in Figure 3.46, where no reduction step characteristic of high oxidation states of gold was observed. The profile is characteristic of iron oxides which are difficult to reduce as only one broad peak is observed at ~430 °C. The fact that gold reduction cannot be identified may suggest that the gold species are already in metallic form after calcination at 560 °C for 6 h. This proposal is supported by the appearance of peaks characteristic of metallic Au in the XRD pattern of this material (see Figure 4.2).

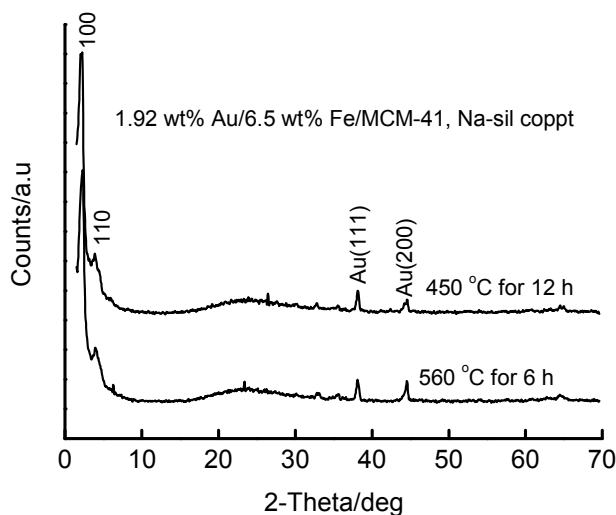


Figure 4.2. XRD patterns of 1.92 wt% Au/6.5 wt% Fe-MCM-41 prepared by direct hydrothermal synthesis at 100 °C for 5 days, from a water-glass coprecipitate of the metal precursors. Prominent metal peaks are indexed in the pattern.

Post-synthesis coprecipitation of the Au(III) and Fe(III) in the presence of precalcined Si-MCM-41 was also investigated as a possible synthesis method for the Au-Fe/MCM-41 materials. The effect of varying the gold content at a fixed Fe content is shown by the XRD patterns of the dried samples in Figure 4.3 (*next page*). This material shows XRD mesoporosity as confirmed by the prominent (100) peak and two higher-order peaks associated with the long-range order of the hexagonal channels. No metal oxide peaks were observed at higher 2θ angles, suggesting that the metal species is highly dispersed in this sample.

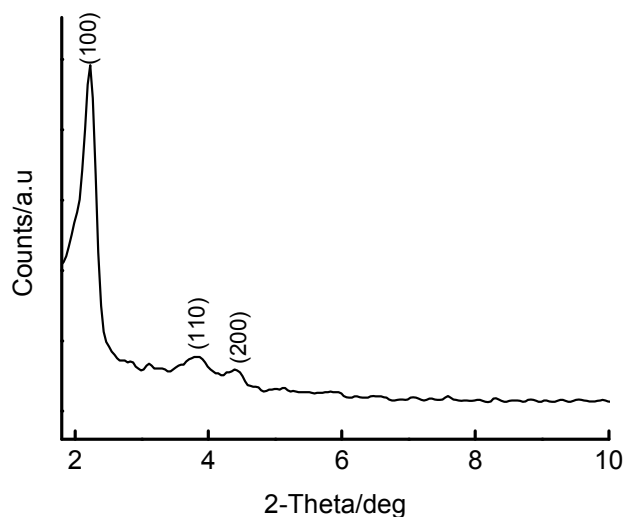


Figure 4.3. XRD pattern of 3 wt% Au/5 wt% Fe/MCM-41 prepared by coprecipitating Au(III) and Fe(III) with a Na_2CO_3 solution in the presence of calcined Si-MCM-41 that was synthesized at 120 °C for 3 days. The material was oven-dried at 120 °C for 15 min prior to XRD analysis.

There seems to be an improvement in structural order of the highly loaded material for materials prepared as above, with varying the Fe content and a fixed Au content (see Figure 4.4 *below*). It can be seen that although both materials show a prominent (100) peak, this peak is less intense and has shifted significantly towards higher 2θ values in the material with the lower total metal content (Figure 4.4(a)). The long-range order is also drastically destroyed as confirmed by the absence of diffraction peaks in the range $3^\circ < 2\theta < 7^\circ$. This observation is contrary to the trend noted for the product formed in the one-pot synthesis, where increased synthesis gel metal content led to inferior mesoporosity of the metal-containing derivatives of MCM-41. Although not conclusive, this observation suggests that the Fe species acts as a nucleation site for the Au, which become well-dispersed on the Fe sites when the concentration of Fe is high and clusters in the pores when little Fe is available for the nucleation of Au. This pore blockage idea is supported by the shift of the (100) peak to higher 2θ values.

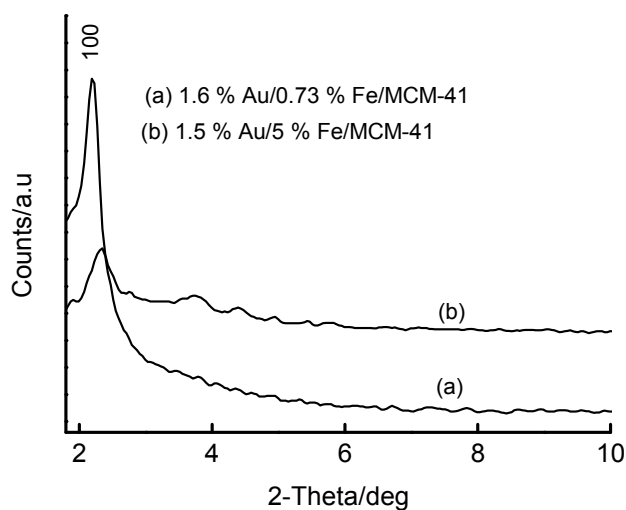


Figure 4.4. XRD patterns of 1.6 wt% Au/0.73 wt% Fe/MCM-41 (a) and 1.5 wt% Au/5 wt% Fe/MCM-41 (b) prepared by coprecipitating Au(III) and Fe(III) with Na_2CO_3 (aq) in the presence of calcined Si-MCM-41 that was synthesized at 120 °C for 3 days. Both materials were air-dried before XRD measurements.

A similar coprecipitation procedure was used to generate materials in the presence of preformed Si-MCM-41 with Co as a base metal. The XRD pattern of the resulting dried and uncalcined material is shown in Figure 4.5 (*next page*). This figure shows a reduction in both mesoporosity (less intense d_{100} peak) and higher order peaks associated with Si-MCM-41. In addition, no metal oxide peaks were observed at high angles, suggesting that the metal species were highly dispersed in the silica matrix.

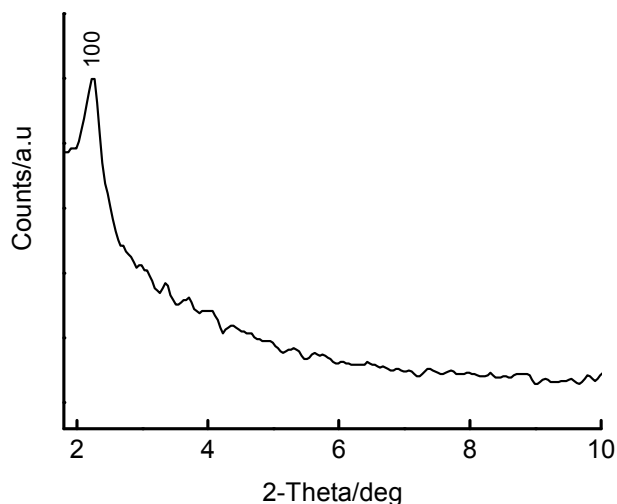


Figure 4.5. XRD pattern of 1.5 wt% Au/5 wt% Co/MCM-41 prepared by coprecipitating Au(III) and Co(II) with Na_2CO_3 (aq) in the presence of preformed Si-MCM-41 that was synthesized at 120 °C for 3 days.

4.3.2. BET Surface Area Measurements

Table 4.2 (*next page*) summarizes the BET surface area data of the Au-containing mesoporous materials prepared in this study. The results show that the final metal-containing materials are mesoporous, with essentially high S_{BET} (comparable with Si-MCM-41) regardless of the preparation method. It is interesting to note that all materials prepared by direct hydrothermal synthesis have specific surface areas reminiscent of the siliceous mesoporous MCM-41. Also noteworthy from Table 4.2 is the high specific surface areas for post synthetically-prepared materials made through heated approaches (homogeneous precipitation with urea and co-DP), as MCM-41 is known to collapse in hot water [86]. This suggests a degree of hydrothermal stability of the supports used, possibly induced by the presence of Fe in the framework. Although the room temperature-synthesized materials show relatively lower BET surface areas than their counterparts prepared under hydrothermal conditions, the surface area associated with Au on Si-MCM-41 ($791 \text{ m}^2/\text{g}$) suggests high surface mobility of Au, culminating in dynamic coalescence

Table 4.2. Variation of S_{BET} for Au/Me-MCM-41 (Me = Si, Co and Fe) with preparation methods and conditions

Comp. (wt% Au) ^a	Prep. Method ^b	Calcination	S_{BET} (m ² /g)
Si-M41	HDT at 80 °C for 6 h	500 °C for 12 h	1225
1.285 Au/Si-M41	HDT at 96 °C for 3 h	500 °C for 12 h	1064
1.36 Au/3 Fe-M41	HDT at 80 °C for 6 h	500 °C for 12 h	1047
2.6 Au/2.96 Fe-M41	HDT at 80 °C for 6 h	500 °C for 12 h	1126
5 Au/Si-M41	PS, (en) route	400 °C for 4 h	791
1 Au/3 Fe-M41	PS, (en) route	400 °C for 4 h	862
5 Au/3 Fe-M41	PS, (en) route	400 °C for 4 h	829
5 Au/5 Fe-M41	PS, (en) route	400 °C for 4 h	825
5 Au/5 Fe-M41	PS, (en) route, IWI with NaBH ₄ /NaOH	400 °C for 4 h	221
5 Au/5 Co-M41	PS, (en) route	400 °C for 4 h	838
3 Au/4.9 Fe-M41	PS, co-DP with NaOH at 85-90 °C for 1 h	400 °C for 4 h	1199
2.67 Au/3 Fe-M41	PS, Homogeneous DP with urea at 90 °C for 1 h	400 °C for 4 h	1091

^a-M41 abbreviates MCM-41

^bHDT means hydrothermal treatment and (en) route means Au(III) was precipitated with aqueous ethylenediamine in the presence of a preformed support at room temperature.

and Au crystallite growth. This results in large Au particles that block some of the pores and reduce the surface area (see TEM micrograph in Figure 4.8). The unusually low S_{BET} for the material prepared by NaBH₄ reduction can be associated with partial destruction of the mesopore lattice by the presence of NaOH in the (NaBH₄-NaOH-H₂O) reducing mixture. The TEM micrograph of this sample (Figure 4.14) also

confirms the significant loss of long-range order. In accordance with our previous observations with Co- and Fe-MCM-41 (Chapter 3) prepared by hydrothermal synthesis, the Co-based materials possess higher surface areas than their Fe-based counterparts (e.g., 5 wt% Au/5 wt% Fe-MCM-41 has $S_{\text{BET}} = 825 \text{ m}^2/\text{g}$ while 5 wt% Au/5 wt% Co-MCM-41 has $S_{\text{BET}} = 838 \text{ m}^2/\text{g}$). The error bar is, however, not significant for these two samples ($\pm 5 \%$).

The Au-containing mesoporous materials with the same amount of Au have been prepared by post-synthesis modification via the ethylenediamine precipitation route in the presence of the preformed Si-MCM-41 or Fe-MCM-41 with varying Fe contents. The S_{BET} of the resulting materials, together with the average particle size of the Au nanoparticles for the 5 wt% Au samples are summarized in Table 4.3 (all calcined at 400 °C for 4 h):

Table 4.3. Surface areas of the Au-containing samples

Metal contents (wt%)	S_{BET} (m^2/g)	Ave. diameter (nm)^a
5 Au/ Si-MCM-41	791	9.9 ± 3.4
5 Au/3 Fe-MCM-41	829	8.8 ± 3.3
5 Au/5 Fe-MCM-41	825	6.9 ± 2.9
5 Au/5 Fe-MCM-41 ^b	221	5.1 ± 3.7

^aThe number after the \pm sign represents the standard deviation of the particle sizes

^bThe material was impregnated with $\text{NaBH}_4/\text{NaOH}/\text{H}_2\text{O}$ before calcination

In chapter 3, it was demonstrated that an increase in the Fe content of the synthesis gel resulted in the formation of materials with lower surface areas than their pure silica counterparts. The above table shows that the incorporation of gold by the post-synthesis technique further decreases the specific surface area of the resulting bimetallic composite. The data can be interpreted by considering the total metal content of each of the samples, i. e., 5, 8 and 10 wt%. There is a close similarity between the

surface area of the material with a total metal content of 8 % and the one containing 10 % metal by weight. The presence of Fe in these materials, although in different amounts, has improved the surface area Si-MCM-41-supported material by 4.6 %. This supports the suggestion made in Table 4.2 above that agglomeration of Au is dominant over siliceous MCM-41, and leads to reduced BET surface areas. Therefore, the weak Au-Si-MCM-41 interactions lead to enhanced sintering with consequent loss of surface area. Also, the incorporation of Fe(III) improves the mechanical properties of Si-MCM-41 and reduces the mobility of Au by creating anchoring sites in the framework. The lowest surface area (221 m²/g) observed after treatment of the 5 wt% Au/5 wt% Fe-MCM-41 with NaBH₄/NaOH/H₂O solution can be attributed to the partial solubility of the SiO₂ component in this alkaline solution. Importantly, the average Au particle size decreases with an increase in the Fe content of the support, signifying the role played by the Fe centres in the support (i.e., numbers of nucleation sites for Au in the support).

4.3.3 High Resolution Transmission Electron Microscopy (HRTEM) Studies

The microstructures of the Au-containing MCM-41 nanocomposite materials prepared via different synthesis routes have been investigated using high resolution transmission electron microscopy (HRTEM). The resulting micrographs enabled the average particle sizes of the Au nanoparticles to be calculated. The particle size distribution (PSD) profiles are also derived from the HRTEM micrographs. The particle size was determined by measuring the diameter of the Au nanoparticles.

4.3.3.1 Gold Incorporation by Direct Hydrothermal Synthesis (One-pot Synthesis)

A monometallic 1.285 wt% Au- MCM-41 was prepared by aging the synthesis mixture at room temperature for 20 hours, treating hydrothermally at 96 °C for 3 h followed by calcination of the material at 500 °C for 12 h. Figure 4.6 (*next page*) shows the HRTEM micrograph and PSD of the resulting material. Large Au crystal-

ites are visible in the micrograph (Figure 4.6 (a)) of these systems. The silica materials are still mesoporous (BET surface area = 1064 m²/g). The PSD profile (Figure 4.6 (b)) shows that most of the nanoparticles have sizes between 19 and 25 nm, and the average particle size is 18 nm. Other nanoparticles with diameters more than 25 nm were also observed. The high average particle sizes of the Au nanoparticles obtained through direct synthesis arises in part from the high calcination temperature (500 °C) needed to decompose the surfactant template, as this temperature is above the Tammann temperature of Au (~395 °C). In light of the particle size expectation for low temperature CO oxidation catalysts, this figure suggests that no room temperature activity can be expected for this material.

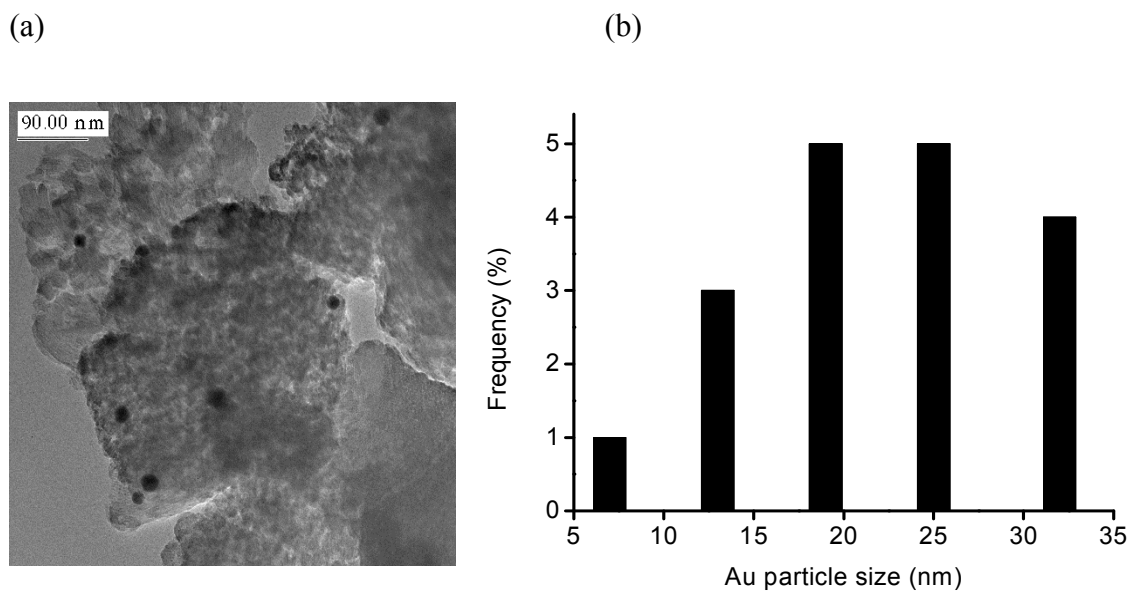


Figure 4.6. HRTEM micrograph (a) and PSD (b) of 1.285 wt% Au/MCM-41 prepared by direct synthesis at 96 °C for 3 h. The synthesis gel was initially aged at room temperature in a PP bottle before carrying out the hydrothermal synthesis, and the final material was calcined at 500 °C for 12 h. Average particle size = 18 nm, standard deviation = 7.

In another *in situ* high-temperature synthesis, a bimetallic 2.59 wt% Au-2.96 wt% Fe/MCM-41 material was prepared from an aqueous mixture of the metal precursors

at 80 °C for 6 h, followed by calcination at 500 °C for 12 h to remove the surfactant template. Figure 4.7 shows a HRTEM micrograph (a) and the PSD (b) of this material. Figure 4.7 (a) shows retention of the structural order of hexagonal pores of the material characteristic of MCM-41 regardless of the presence of Au precursors during synthesis. Analogous to the observations in Figure 4.6, the direct hydrothermal synthesis of Au-containing mesoporous materials is accompanied by the formation of large gold nanoparticles, owing primarily to the high calcination temperatures used (≥ 500 °C). The average particle size of the Au nanoparticles in this material is 23 nm. Again, on the basis of the particle size requirement for low-temperature CO oxidation activity, this method is not viable for preparing highly active catalysts. Therefore, alternative synthetic approaches were investigated in order to prepare catalysts with smaller particles sizes. In an attempt to achieve this, preformed mesoporous supports were first prepared and the gold precursors introduced post-synthetically to avoid the need to calcine the materials at ≥ 500 °C.

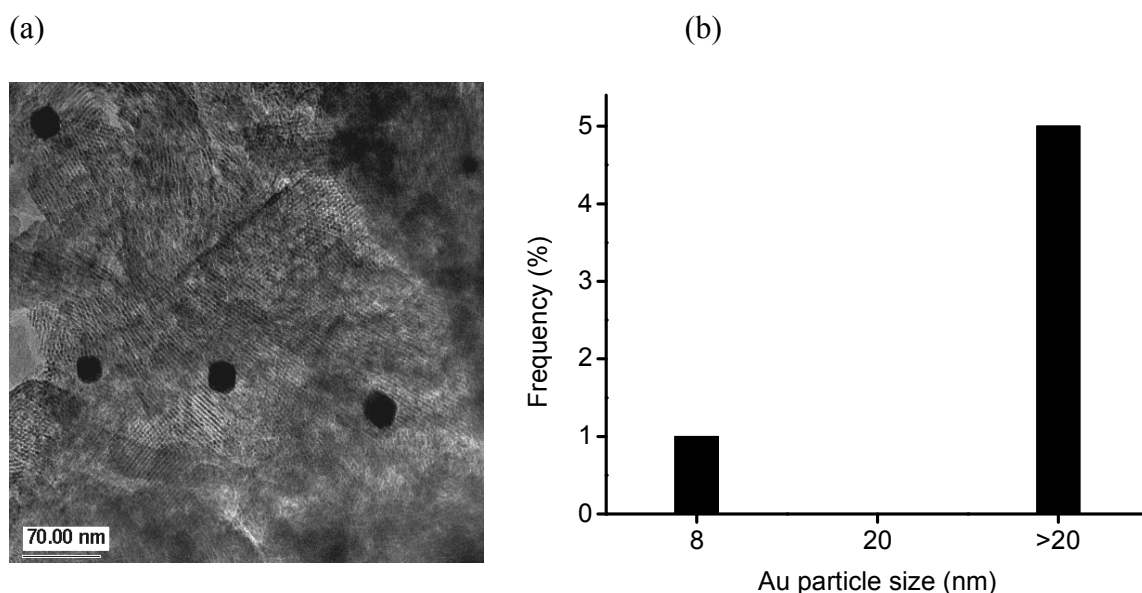


Figure 4.7. HRTEM image (a) and particle size distribution (b) of 2.6 wt% Au/2.96 wt% Fe-MCM-41 prepared in situ at 80 °C for 6 h and calcined at 500 °C for 12 h. Average particle size = 23 nm, standard deviation = 8.

4.3.3.2 Post-synthesis Incorporation of Au in Mesoporous Supports

In this approach, use was made of a preformed support material which has been previously calcined to remove the template. The support materials were either Si-, Fe- or Co-MCM-41 prepared by one-pot synthesis. This method offers the advantage of activating or calcining the resulting gold-containing materials at low temperatures. The results of different post-synthesis preparations are discussed below.

4.3.3.3 Gold Incorporation by Precipitation with ethylenediamine solution and calcination

Figure 4.8 below illustrates the HRTEM micrograph and the Au particle size distribution (PSD) of the 5 wt% Au/Si-MCM-41 material prepared by this method:

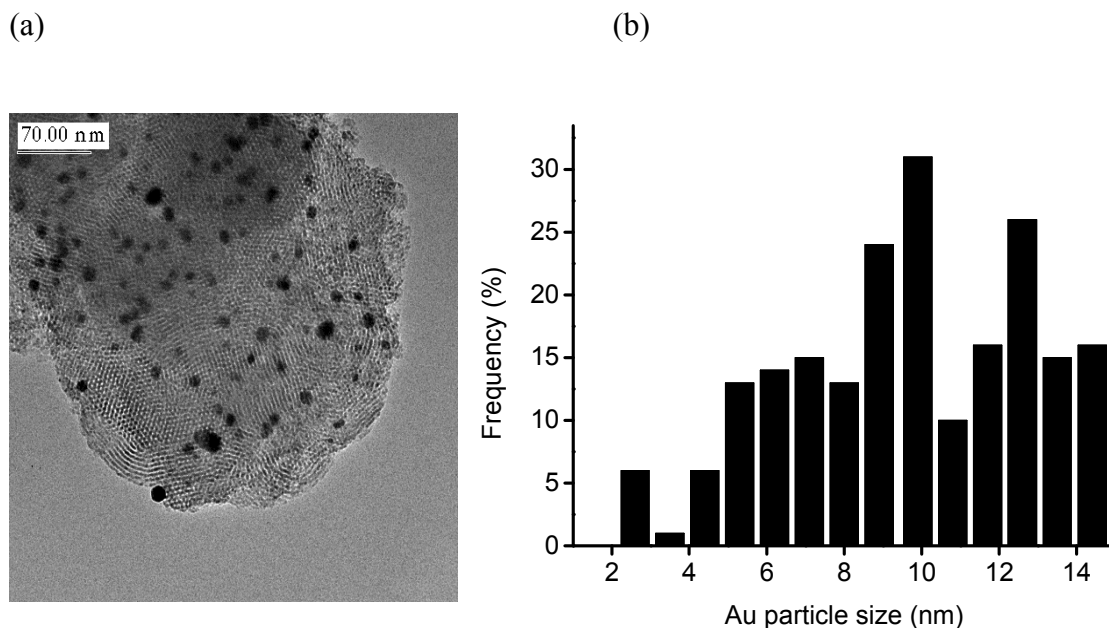


Figure 4.8. HRTEM image (a) and PSD (b) of 5 wt% Au/Si-MCM-41 prepared by precipitating Au(III) with (en) solution in the presence of calcined Si-MCM-41, calcined at 400 °C for 4 h. Average particle size = 10 nm, standard deviation = 3.

It is evident from Figure 4.8 that this synthetic approach retains a greater percentage of the hexagonally ordered pore structure of Si-MCM-41 (cf. parent material in chapter 2). This structural retention stems from the use of an already ordered support material, coupled with the relatively lower calcination temperatures (compared to those used to remove the surfactant in the one-pot synthesis method). The Au particle size distribution shows that the majority of the particles are in the 9-13 nm size range, with an average diameter of 10 nm. Thus, on siliceous MCM-41, predominantly large Au particles result after calcination at 400 °C and are spread all over the surface of the mesoporous material (Figure 4.8). The increased size of the Au particles can be attributed to the increased surface mobility of Au at the calcination temperature (400 °C), due to weak gold-Si-MCM-41 interactions.

In a similar synthesis, Si-MCM-41 was replaced by preformed 3 wt% Fe-MCM-41 as a support for Au nanoparticles. Figures 4.9 – 4.11 show the HRTEM micrographs and PSD profiles for the resulting materials with Au contents ranging from 1 to 5 wt%. The Au-containing material in Figure 4.9 (*next page*) also shows retention of mesoporous long-range order similar to that of the parent support (see Figure 3.29). This may be a result of the low Au loading and the relatively lower calcination temperature used. The average particle size of the Au nanoparticles is (6 ± 4) nm, which is larger than the limit required for high low-temperature catalytic activity.

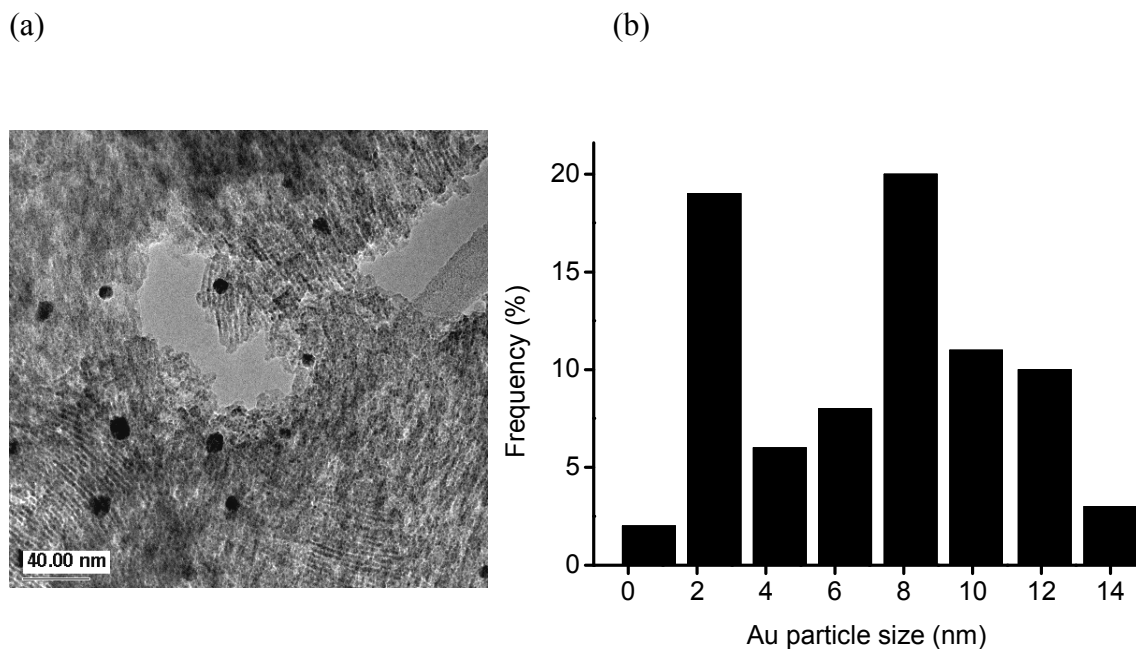


Figure 4.9. HRTEM image (a) and PSD (b) of 1 wt% Au/3 wt% Fe-MCM-41 prepared by precipitating Au(III) with en solution in the presence of calcined 3 wt% Fe-MCM-41, calcined at 400 °C for 4 h. Average particle size = 6 nm, standard deviation = 4.

Increasing the Au loading to 2.57 wt% following the same method outlined above shows improved dispersion of the Au species on the Fe-premodified support as shown in Figure 4.10.

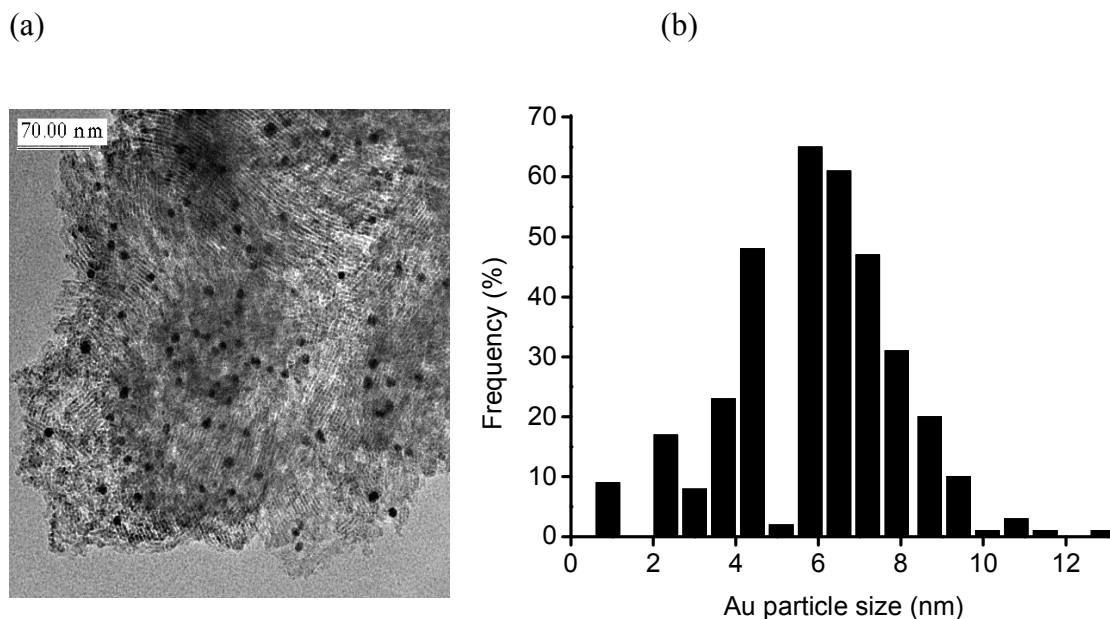


Figure 4.10. HRTEM image (a) and PSD (b) of 2.57 wt% Au/3 wt% Fe-MCM-41 prepared by precipitating Au(III) with en solution in the presence of calcined 3 wt% Fe-MCM-41, calcined at 400 °C for 4 h. Average particle size = 6 nm, standard deviation = 2.

Also noteworthy from Figure 4.10 is the fact that the particle size is well controlled by the presence of a base metal in the support, with most of the particles between 6 and 7 nm in size, and the average particle diameter of (6 ± 2) nm. However, the MCM-41-type order is still visible in the micrograph of this material.

A further increase in the Au content to obtain 5 wt% Au/3 wt% Fe-MCM-41 by the same approach, led to the HRTEM and PSD shown in Figure 4.11.

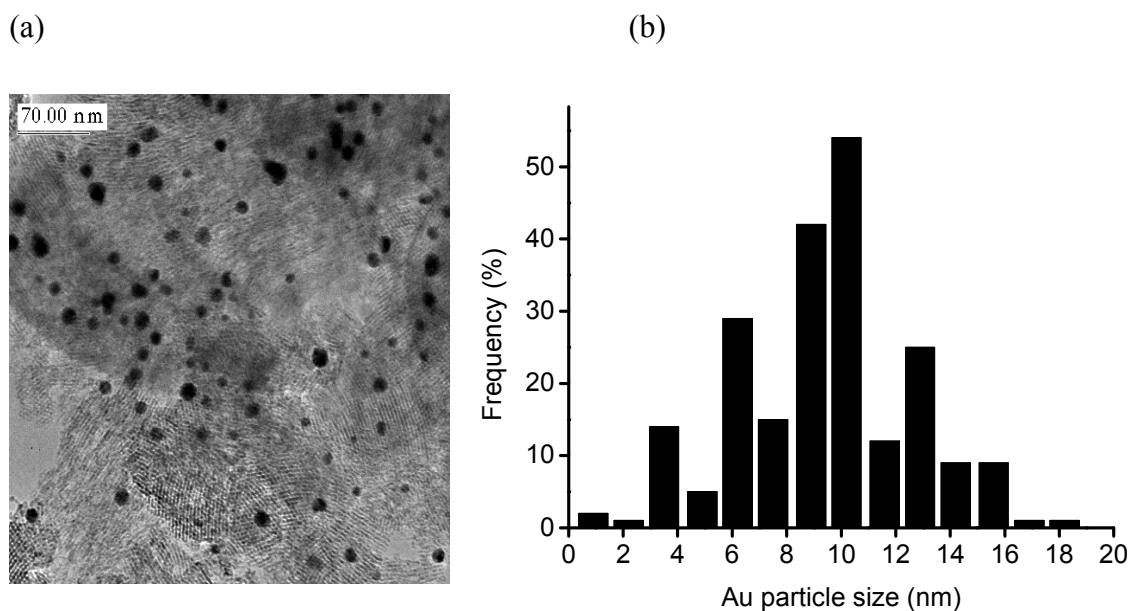


Figure 4.11. HRTEM image (a) and PSD (b) of 5 wt% Au/3 wt% Fe-MCM-41 prepared by precipitating the Au(III) with en solution in the presence of calcined 3 wt% Fe-MCM-41, calcined at 400 °C for 4 h. Average particle size = 9 nm, standard deviation = 3.

Figure 4.11 shows the presence of relatively larger gold particles (average diameter of 9 nm) than those observed in the 2.57 wt% Au/3 wt% Fe-MCM-41 material in Figure 4.10. This difference may stem from the shortage of nucleation sites (the Fe centres) in a highly loaded 5 wt% Au material, leading to dynamic coalescence or Ostwald ripening of the Au nanoparticles during the calcination step. Note that the MCM-41 type structure is still present in the support at this loading, although over shorter domains.

A 5 wt% Au/5 wt% Fe-MCM-41 material has been prepared similarly to the 5 wt% Au/3 wt% Fe-MCM-41 material above (i.e., following the en deposition-precipitation route) in order to elucidate the effect of the Fe content in the support. Figure 4.12 below shows the HRTEM micrograph and the PSD profile of the resulting calcined material.

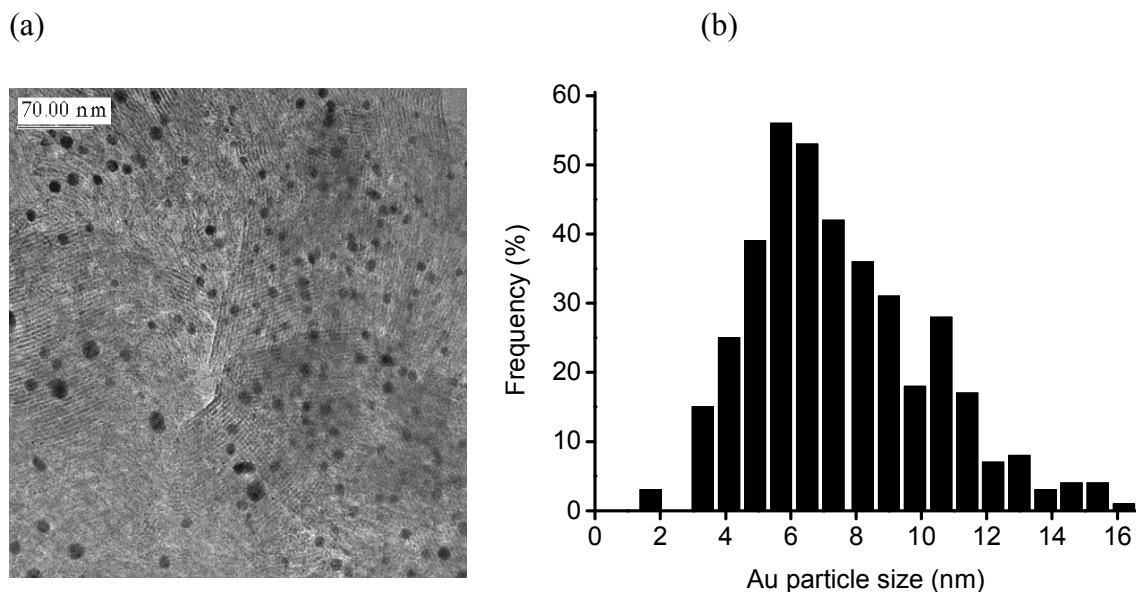


Figure 4.12. HRTEM image (a) and PSD (b) of 5 wt% Au/5 wt% Fe-MCM-41 prepared by precipitating Au(III) with en solution in the presence of calcined 5 wt% Fe-MCM-41, followed by calcination at 400 °C for 4 h. Average particle size = 7 nm, standard deviation = 3.

In addition to the retention of high structural order of the mesostructure, the individual Au particles on the micrograph of this material are relatively smaller than those in the material based on 3 wt% Fe-MCM-41 (Figure 4.11). The PSD profile (Figure 4.12 (b)) has a log-normal shape, which shows an improvement in the particle size distribution of the material. The majority of the Au particles have diameters of about ≤ 6.5 nm, while the majority of the Au particles for the corresponding material based on 3 wt% Fe-MCM-41 had diameters in the range 9 -10 nm. This lowering in the average particle size of Au nanoparticles with increased base-metal content in the support material may suggest that there are more nucleation sites in 5 wt% Fe-MCM-41 than there are in 3 wt% Fe-MCM-41, and consequently less agglomeration of Au particles in the former.

A 5 wt% Au/5 wt% Fe-MCM-41 material was prepared via the ethylenediamine precipitation route of Au(III) in the presence of pre-formed 5 wt% Fe-MCM-41. After the washing and drying treatments, the material was impregnated to incipient wetness with a reducing alkaline/basic solution of composition 0.27 % NaBH₄/ 0.89 % NaOH/ 8.85 % H₂O, dried and calcined at 400 °C for 4 h. The HRTEM characteristics of the resulting material are shown in Figure 4.13.

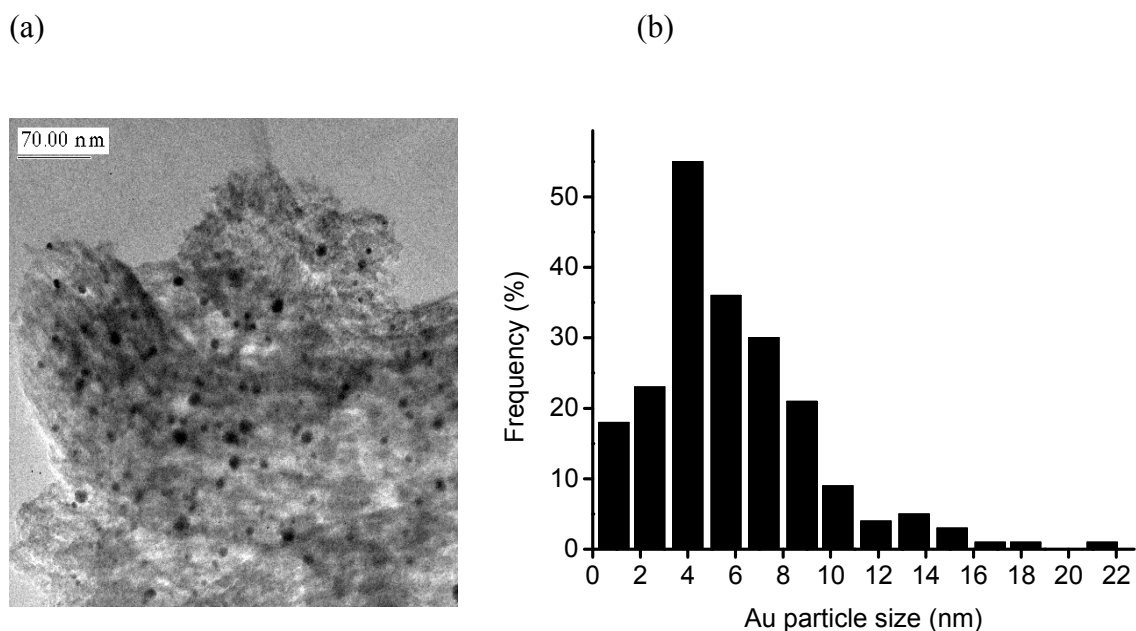


Figure 4.13. HRTEM image (a) and PSD (b) of 5 wt% Au/5 wt% Fe-MCM-41 prepared by precipitating Au(III) with en solution in the presence of preformed 5 wt% Fe-MCM-41, then treated to incipient wetness with a dilute base solution (0.27 % NaBH₄/0.89 % NaOH/8.85 % H₂O) prior to calcination at 400 °C for 4 h. Average particle size = 5 nm, standard deviation = 4.

Besides the partial loss of the long-range order of the support matrix (Figure 4.13 (a)), probably due to impregnation with a reducing alkaline solution, the material exhibits a good distribution profile (log-normal type). The majority of the Au nanoparticles have a diameter of 4 nm, and the average particle size is 5 nm, which is ~27 % smaller than the corresponding material without basic reductive treatment

(Figure 4.12 above). The sodium borohydride treatment was employed since gold nanoparticles particles can be generated in solution by reduction with solutions containing NaBH_4 [87, 88], and BoroMet 1240 (an aqueous solution of NaBH_4 and NaOH) [89]. Boromet is used in the reduction and recovery of precious metals [89]. Thus, the effect of the $\text{NaBH}_4/\text{NaOH}$ treatment was to reduce the particle size of the resulting Au nanoparticles.

The ethylenediamine synthesis route has also been applied in the preparation of a 5 wt% Au-containing material prepared in the presence of 14 wt% Fe-MCM-41 (itself prepared by in situ hydrothermal treatment). The HRTEM micrograph (a) and PSD (b) of this material is shown in Figure 4.14.

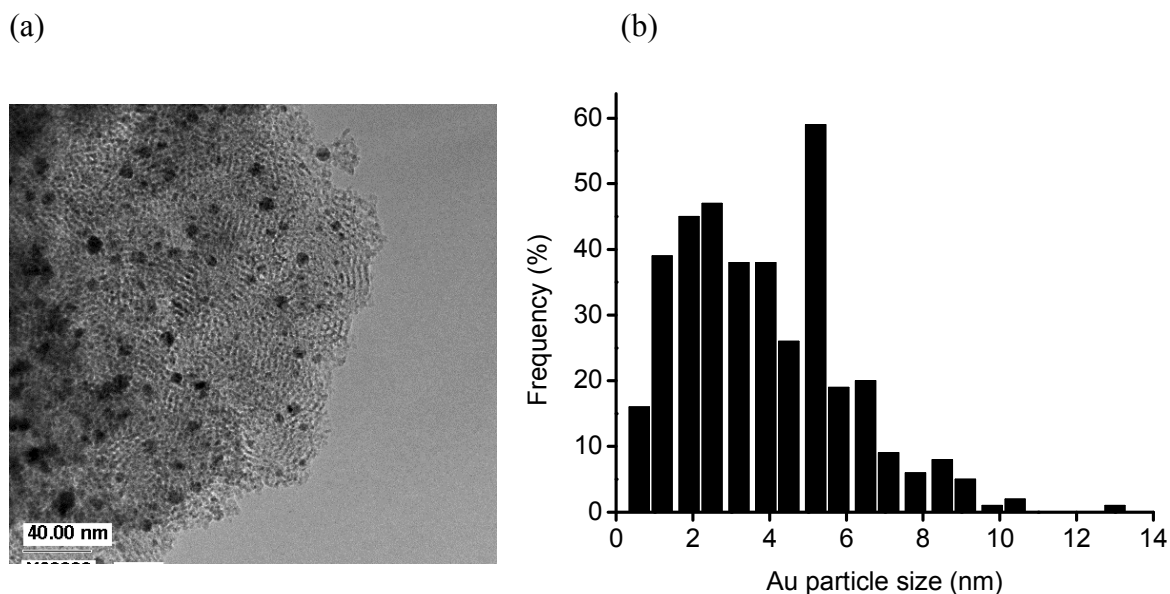


Figure 4.14. HRTEM image (a) and PSD (b) of 5 wt% Au/14 wt% Fe-MCM-41 prepared by precipitating Au(III) with en solution in the presence of calcined 14 wt% Fe-MCM-41, followed by calcination at 380 °C for 6 h. Average particle size 4 nm, standard deviation = 2.

Figure 4.14 above shows that in spite of the high Fe content of the support (14 wt% Fe-MCM-41), the porous structure of MCM-41 is preserved, even after introducing

the Au species. Both large and small Au particles are evident in the micrographs of the sample above. From the PSD profile of this material, given below, it is evident that most of the Au particles have diameters ≤ 5 nm. The average particle size of the Au nanoparticles in this sample is 3.6 nm. There are many nucleation sites that may be associated with the Fe content of the support and this decreases the chances of excessive agglomeration of the Au particles. The low temperature at which this material was calcined can also be assumed to minimize surface mobility of the Au species.

Cobalt-derivatized MCM-41 has also been investigated as a possible support for the Au nanoparticles prepared via the ethylenediamine precipitation of Au. Figure 4.15 (*next page*) shows the HRTEM micrograph and the PSD of calcined 1 wt% Au/5 wt% Co-MCM-41 prepared in the presence of preformed 5 wt% Co-MCM-41.

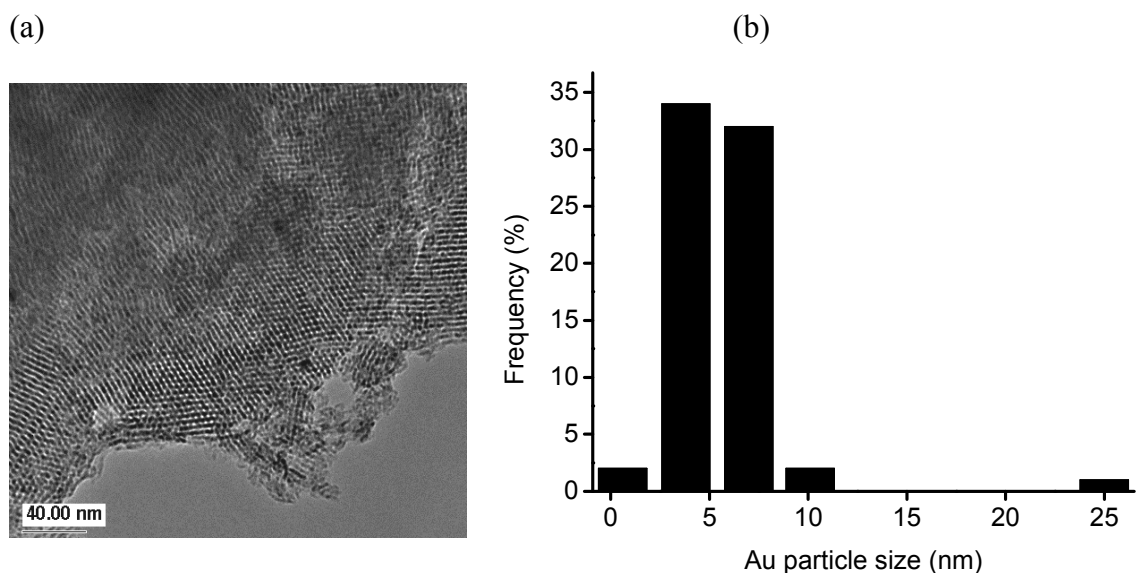


Figure 4.15. HRTEM image (a) and PSD (b) of 1 wt% Au/5 wt% Co-MCM-41 prepared by precipitating Au(III) with en solution in the presence of 5 wt% Co-MCM-41, followed by calcination at 400 °C for 4 h. Average particle size = 4 nm, standard deviation = 3.

The above figure shows that the resulting material is highly ordered and exhibits characteristics reminiscent of Si-MCM-41. This retention of regularity in the pore structure may be associated with the low Au loading in the final calcined material. The PSD profile show that most of the Au nanoparticles have diameters of 4 and 7 nm, and the average particle size is 4 nm.

Following the synthetic approach above, a 5 wt% Au/5 wt% Co-MCM-41 was prepared by precipitation of the Au(III) with 1 M ethylenediamine solution in the presence of pre-formed 5 wt% Co-MCM-41. Figure 4.16 shows the HRTEM micrograph and the corresponding PSD profile for the resulting material after calcination.

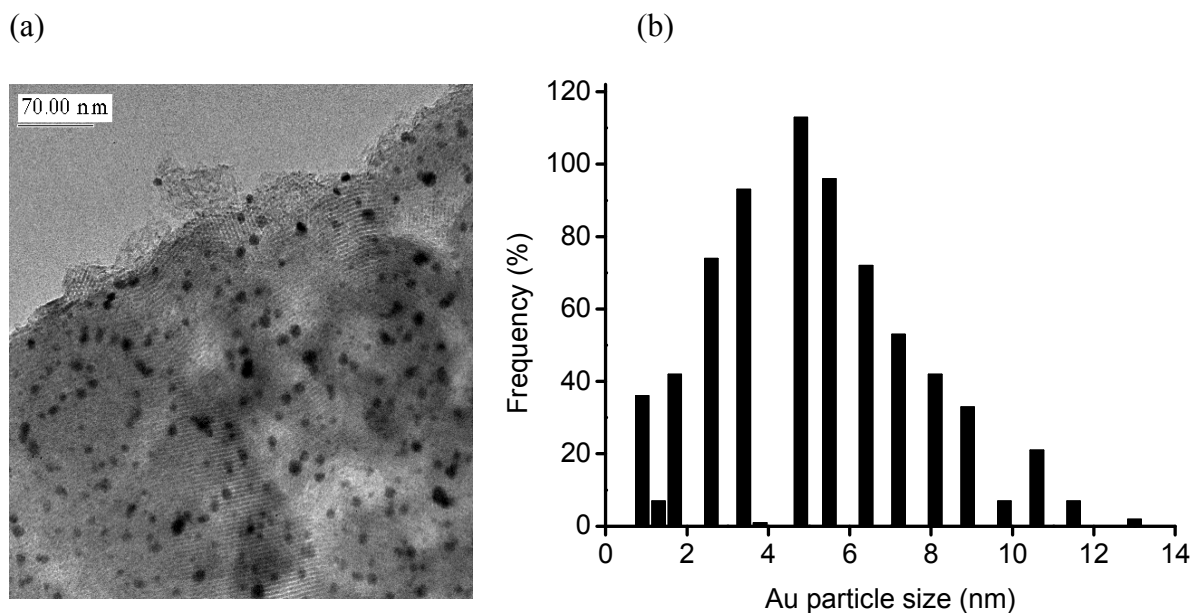


Figure 4.16. HRTEM image (a) and PSD (b) of 5 wt% Au/5 wt% Co-MCM-41 prepared by precipitating Au(III) with en in the presence of preformed 5 wt% Co-MCM-41, calcined at 400 °C for 4 h. Average particle size is 5 nm and standard deviation is 2.

As seen from the figure above, the presence of 5 wt% Co in the mesoporous support improves the distribution of gold nanoparticles and leads to relatively smaller

particles than those obtained in the presence of 5 wt% Fe. The majority of the nanoparticles are in the 3.5 - 6 nm size range, with the average diameter of 5 nm.

4.3.3.4 Gold Incorporation by Other Methods (Post-synthetically)

In a modified ethylenediamine precipitation route discussed above, the HAuCl_4 aqueous solution was stirred for 1 hour with the surfactant containing Si-MCM-41, with the aim of inducing electrostatic interactions between the AuCl_4^- anion and the CTA^+ cation occluded in the pores of the as-synthesized material. After treatment with the (en) solution to precipitate the Au(III) precursor in the pores, the dried material was studied by HRTEM and the results are shown in Figure 4.17.

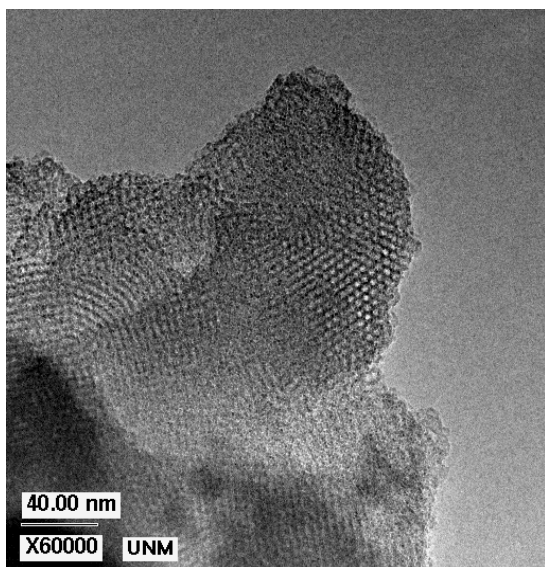


Figure 4.17. The HRTEM image of 2.28 wt% Au/CTAB-Si-MCM-41 prepared by ethylenediamine precipitation of Au(III). The material is in its uncalcined state.

It can be seen from Figure 4.17 above that the material is highly ordered and shows a microstructure characteristic of Si-MCM-41. The gold nanoparticles were not clearly visible and did not allow measurement of their diameters. This can be taken as evidence that the majority of the gold species is present *inside* the channels as a result

of the affinity of the anionic Au species for the cationic surfactant template in the pores.

However, upon calcination of the material in Figure 4.17 at 500 °C for 12 h, gold nanoparticles appear on the surface of the material as the cationic surfactant is burnt off. The gold particles migrate to the surface as a result of the weak Au-SiO₂ interactions. Note that high temperatures were needed since the support still contained the surfactant template. The resulting gold nanoparticles are relatively large as a result of this high calcination temperature used to decompose the surfactant template. Figure 4.18 illustrates this effect of calcination on the TEM microstructure of this material.

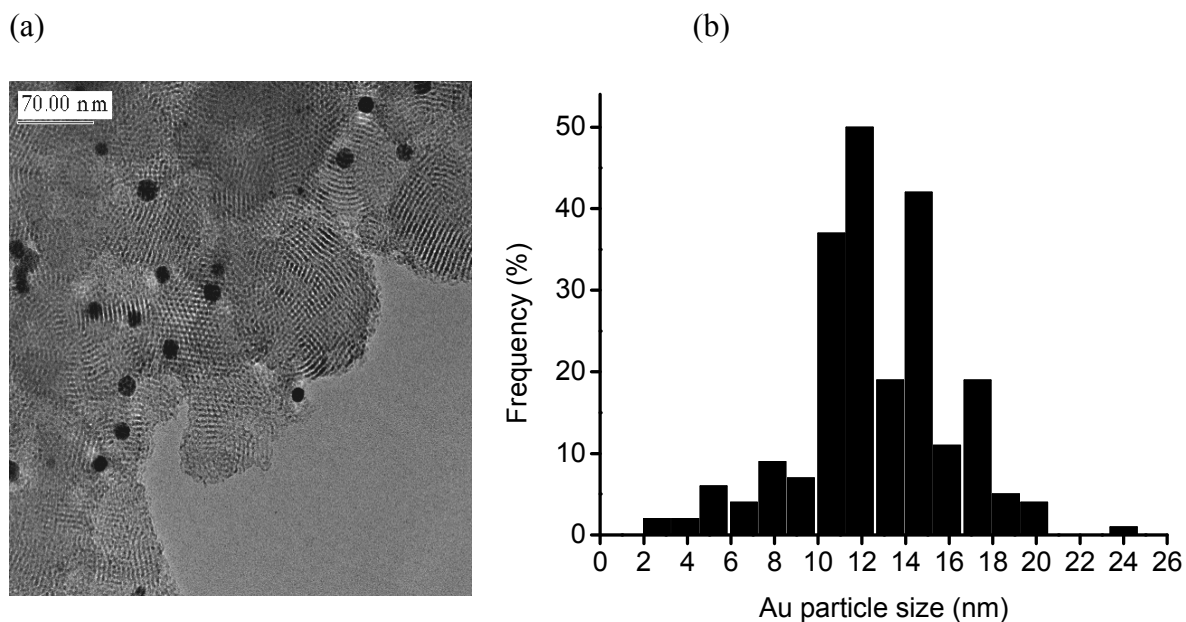


Figure 4.18. HRTEM image (a) and PSD (b) of 2.28 wt% Au/CTAB-Si-MCM-41 prepared by precipitating Au(III) with en solution in the presence of the as-synthesized Si-MCM-41, followed by calcination at 500 °C for 12 h. Average particle size is 12 nm and standard deviation is 3.

Importantly, the material retained much of the long-range order even after calcination, but the draw-back associated with this synthesis approach is the relatively large Au particles obtained. The presence of the template in the mesopores during the incorporation of Au seems to play a role of maintaining the high order of the channel structure, although it easily leads to sintering of the Au particles as seen from the above micrograph. The particle size distribution profile shows that the majority of the gold nanoparticles are in the 11 -15 nm size range, with the average diameter of 12 nm. Regardless of the difference in gold loadings between this material and the 5 wt% Au-containing material prepared with pre-calcined Si-MCM-41, the effect of the high calcination temperature is highlighted and coupled to the weak Au-SiO₂ interactions.

A 2.67 wt% Au/3 wt% Fe-MCM-41 material has been prepared by applying the ideas of homogeneous precipitation of the Au(III) by using urea. This was achieved by heating the Au(III)/urea solution at 90 °C for 1 h in the presence of pre-formed 3 wt% Fe-MCM-41. This is once again reminiscent of the deposition precipitation method. After washing the material to a negative Cl⁻ ion test and drying at ambient temperature, it was calcined at 400 °C for 4 h. Figure 4.19 (*next page*) shows the HRTEM micrograph and the PSD profile of the resulting material. Figure 4.19 shows decreased long-range order of the support material (see parent support in Figure 3.29) due to the confluence of the increased basicity of the slurry upon decomposition of urea in aqueous solutions, and the hydrothermal instability of MCM-41-type materials [90]. However, the structural collapse due to hydrothermal instability may not be significant as He et al [91, 92] detected little collapse of silica following the incorporation of La³⁺ and Fe³⁺ into the MCM-41 framework. Therefore, the major factor leading to the observed decrease in the long-range order of the Au-containing material above should be the partial solubility of the silica in alkaline media. Interestingly, the Au nanoparticles obtained by this route are relatively small, with the PSD profile showing that the majority of the nanoparticles are in the 2 - 4 nm size range.

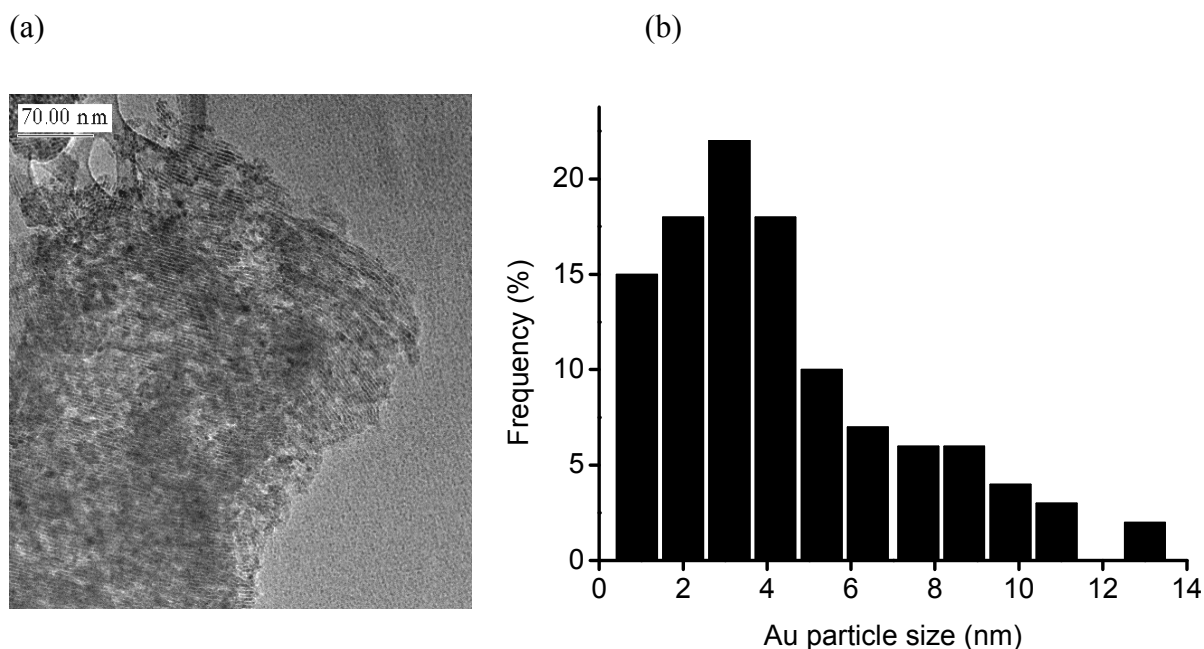


Figure 4.19. HRTEM image (a) and PSD (b) of 2.67 wt% Au/3 wt% Fe-MCM-41 prepared by precipitating Au(III) with urea in the presence of 3 wt% Fe-MCM-41, calcined at 400 °C for 4 h. Average particle size is 4 nm and standard deviation is 3.

Synthesis of 1.1 wt% Au on 3 wt% Fe-MCM-41 by reduction of the Au(III) with trisodium citrate solution at 70-80 °C gave very small Au particles on the mesoporous support after calcination at 325 °C for 6 h (see Figure 4.20, *next page*). Figure 4.20 (a) shows no significant loss of the long-range order in the pore structure of the support (see parent support in Figure 3.29). Furthermore, although the PSD (Figure 4.20 (b)) does not follow a log-normal distribution, it confirms that the resulting Au particles are very small as the majority fall in the size range 1-2 nm. This is not surprising as the trisodium citrate reduction of Au(III) in water is a well-documented method for the preparation of colloidal gold nanoparticles, and produces gold particles with a narrow size distribution [93 - 95]. This is confirmed by the average particle size of 2 nm obtained for the resulting supported Au sample prepared by this route (see Table 4.4 (c)).

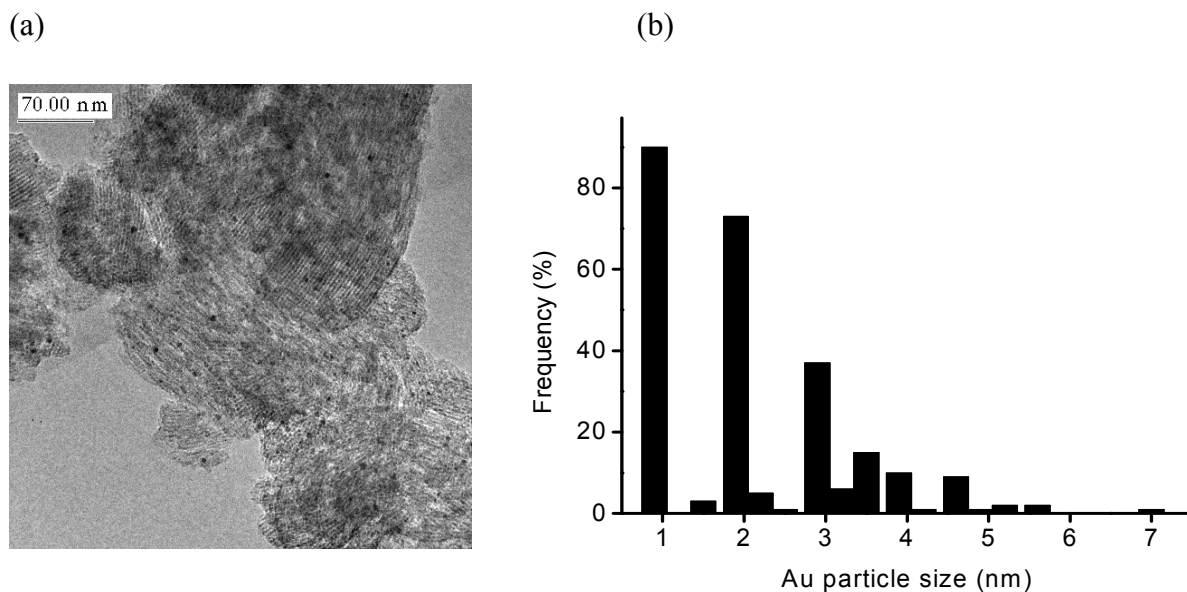


Figure 4.20. HRTEM image (a) and PSD (b) of 1.1 wt% Au/3 wt% Fe-MCM-41 prepared by reducing Au(III) with sodium citrate in the presence of calcined 3 wt% Fe-MCM-41, calcined at 325 °C for 6 h. Average particle size is 2 nm, standard deviation is 1.

A summary of the HRTEM data, in which samples are grouped according to the synthesis methods, is given in Tables 4.4 (a)-(c).

Table 4.4 (a). One-pot synthesized Au-containing materials calcined at 500 °C for 12 h.

Composition (wt%)	Synthesis conditions	Average particle size (nm)
1.285 Au/Si-MCM-41	96 °C for 3 h	18 ± 7
2.59 Au/2.96 Fe-MCM-41	80 °C for 6 h	23 ± 8

Table 4.4 (b). Post-synthetically prepared Au-containing MCM-41 prepared via en route. Calcination was done at 400 °C for 4 h, unless stated otherwise in the footnote.

Composition (wt%)	Synthesis conditions	Average particle size (nm)
<i>Si-MCM-41 supports</i>		
2.28 Au/CTA-Si-MCM-41	(en) route at RT ^a	12 ± 3
5 Au/Si-MCM-41	(en) route at RT	10 ± 3
<i>Fe-MCM-41 support</i>		
1 Au/3 Fe-MCM-41	(en) route at RT	6 ± 4
2.57 Au/3 Fe-MCM-41	(en) route at RT	6 ± 2
5 Au/3 Fe-MCM-41	(en) route at RT	9 ± 3
5 Au/5 Fe-MCM-41	(en) route at RT	7 ± 3
5 Au/5 Fe-MCM-41	(en) route at RT ^b	5 ± 4
5 Au/14 Fe-MCM-41	(en) route at RT ^c	4 ± 2
<i>Co-MCM-41 supports</i>		
1 Au/5 Co-MCM-41	(en) route at RT	4 ± 3
5 Au/5 Co-MCM-41	(en) route at RT	5 ± 2

^aMaterial calcined at 500 °C because it still contains the surfactant (CTA)

^bMaterial treated with NaBH₄/NaOH/H₂O solution before calcination

^cMaterial calcined at 380 °C for 6 h.

Table 4.4 (c). Other post-synthesis methods for Au-containing materials

Composition (wt%)	Synthesis conditions	Average particle size (nm)
2.67 Au/3 Fe-MCM-41	Urea precipitation at 90 °C ^a	4 ± 3
1.1 Au/3 Fe-MCM-41	Sodium citrate reduction ^b	2 ± 1

^aCalcined at 400 °C for 4 h

^bCalcined at 325 °C for 6 h

Tables 4.4 (a) – 4.4 (c) show that:

One-pot Synthesis: Large particles are formed as a result of the need to decompose the surfactant template (calcine at 500 °C). The largest average particle size in the Fe-containing nanocomposite may suggest that Fe promotes Au cluster nucleation and crystal growth in this material.

Ethylenediamine route: Si-MCM-41 based materials produce large Au particles primarily due to weak gold-support interactions. The large size is more pronounced in the template-containing support as a result of the high calcination temperature requirement.

Fe-MCM-41 based materials showed that increasing the Au content at a fixed Fe content in the support is accompanied by crystal growth (probably due to sintering). For the sample based on 5 wt% Fe-MCM-41, NaBH₄/NaOH/H₂O treatment causes a partial reduction in the Au particle size.

Co-MCM-41 based materials exhibit smaller average gold particle sizes than the corresponding Fe-MCM-41 based materials.

Other post-synthesis methods: These produced Au-containing materials with a pronounced reduction in the average particle size of the Au nanoparticles.

4.4. Conclusions

In this chapter, we have presented the synthesis of mesoporous gold-silica nanocomposites through a one-step sol-gel reaction using CTAB as a pore structure directing template. The S_{BET} , Au particle size distribution and pore structure of the nanocomposites formed can be fine-tuned by manipulating the synthesis methods and parameters. Therefore, in the presence of CTAB as template, mesoporous gold-MCM-41 nanocomposite materials were successfully prepared using the sol-gel process, i.e., combining gold sol and prehydrolyzed silica sol.

The bimetallic composite material 1.92 wt% Au/6.5 wt% Fe-MCM-41 synthesized in situ at 100 °C for 5 days from a water-glass coprecipitate and CTAB showed retention of XRD mesoporosity. On calcination, these materials revealed the presence of metallic gold in the high-angle region of the XRD patterns in addition to the mesostructure. The presence of metallic gold has also been confirmed by TPR studies, which showed no reduction peak characteristic of ionic gold. Only one reduction peak was observed at $T_{\text{max}} = 427$ °C and this can be attributed to the reduction of the Fe species in intimate contact with the silica matrix (see Chapter 3). Notably, the XRD studies did not reveal the presence of Fe-related species, regardless of the higher Fe content in this material, and this may be diagnostic evidence that the Fe species is highly dispersed. Calcination converts ionic Au to metallic Au.

Both 1-pot synthesis and post-synthesis pathways produced materials with surface areas reminiscent of mesoporous materials. The advantage of post-synthesis metal incorporation is the opportunity to start with an already ordered material, hence higher loadings are possible without serious disruption of the long-range order. Post-synthesis modification of calcined Si-MCM-41 with low Au contents results in the formation of discrete gold particles of fairly uniform size, scattered randomly on the surface. Atomically dispersed Fe and Co improves the dispersion of gold throughout the surface of the mesostructure. Also, the destructive effect of Au on the MCM-41

framework was significantly prevented by the presence of the base metal component in the support material (see Table 4.3). Aggregation of Au clusters and the reduction in the BET surface area were more pronounced on Si-MCM-41 as a result of sintering during the calcination step (i.e., weak interactions between Au and Si-MCM-41). However, aggregation is not widespread, and most of the gold particles exist as isolated species.

In general, the presence of base metals in the support materials improves the particle size and the distribution of Au nanoparticles, leading to a log-normal particle size distribution in most samples. It thus seems probable to presume that base metals in the support provide anchors or nucleation sites for the Au nanoparticles, and retard their surface mobility at the calcination temperatures.

A number of deductions follow from this study:

- 1) Direct hydrothermal synthesis of the Au-containing mesoporous materials is unsuitable for the preparation of Au nanoparticles in the size range capable of catalyzing CO oxidation at low temperatures, a feature arising from the need to calcine the final materials at $T_{\text{calc.}} \geq 500$ °C. The largest average particle size of Au in the Au-Fe-MCM-41 nanocomposite material may suggest that Fe promotes nucleation and crystal growth in this synthesis approach.
- 2) Post-synthesis incorporation of Au, starting with a preformed calcined support material before introducing Au precursors, allows the use of lower activation temperatures and offers the advantage of retaining most of the long-range order of the mesoporous support. Also, the relative sizes of the Au nanoparticles are lower in materials made by post-synthesis methods as compared to hydrothermally-derived materials.

3) Although the material prepared by direct hydrothermal synthesis with both the Fe and the Au precursors as part of the initial synthesis gel had a reasonably high surface area, HRTEM showed agglomeration of Au, most probably resulting from the high calcination temperature required to remove the surfactant template. The high BET surface areas for materials obtained through heated post-synthesis techniques (e.g., co-deposition-precipitation with NaOH and homogeneous deposition-precipitation using urea) suggest good hydrothermal stability of the materials used as supports.

4) Homogeneous precipitation with urea gives a good PSD profile of the metal particles, with the average particle diameter in the range associated with low temperature CO oxidation activity.

5) Reduction with tri-sodium citrate produced Au nanoparticles with the smallest average diameter of all the samples prepared in this study.

6) Incipient wetness impregnation of the 5 wt% Au/5 wt% Fe-MCM-41, prepared by the (en) precipitation of Au(III) onto 5 wt% Fe-MCM-41, with a reducing solution of NaBH₄/NaOH/H₂O prior to calcination resulted in a normal distribution of Au nanoparticles and a smaller average diameter than the corresponding material in which no reduction treatment was used.

7) Preparation with the as-synthesized Si-MCM-41 material offers a good alternative for getting the majority of the Au inside the channels of MCM-41, as the occluded cationic surfactant template interacts strongly with the anionic Au precursor, AuCl₄⁻. However, this method suffers a drawback because high temperatures (≥ 500 °C) are required to remove the surfactant, as in the one-pot synthesis. These high calcination temperatures promote agglomeration and sintering of the Au nanoparticles because the metal-support interactions between Au and SiO₂ are weak, and the surface mobility of the Au species is enhanced.

8) Regardless of the method of preparation of the Au-containing mesoporous materials reported in this study, the specific surface areas remain essentially high. Low surface areas are typically observed for materials prepared on unmodified supports, where particle growth is pronounced and pore blockage is likely to take place. For the same Au loading and base metal content (Fe or Co), the Co-MCM-41-based materials possessed higher BET surface areas than the Fe-based materials. HRTEM studies have also shown the former materials to contain relatively smaller Au crystallites than the latter.

4.5 References

1. J. Schwank, *Gold Bull.* **16**, 103 (1983)
2. B. Hammer and J. K. Norskov, *Nature* **376**, 238 (1995)
3. G. J. Hutchings, *J. Catal.* **96**, 292 (1985)
4. M. Haruta, T. Kobayashi, H. Sano and N. Yamada, *Chem. Lett.* 405 (1987)
5. M. Haruta and M. Date, *Appl. Catal. A: Gen.* **222**, 427 (2001)
6. M. Haruta, N. Yamada, T. Kobayashi and S. Iijima, *J. Catal.* **115**, 301 (1989)
7. M. Haruta, S. Tsubota, T. Kobayashi, H. Kageyama, M. J. Genet and B. Delmon, *J. Catal.* **144**, 175 (1993)
8. G. C. Bond, *Catal. Today* **72**, 5 (2002)
9. C. M. Yang, M. Kalwei, F. Schuth and K.-J. Chao, *Appl. Catal. A: Gen.* **254**(2), 289 (2003)
10. T. M. Salama, R. Ohnishi, T. Shido and M. Ichikawa, *J. Catal.* **162**, 169 (1996)
11. T. Hayashi, K. Tanaka and M. Haruta, *J. Catal.* **178**, 566 (1998)
12. B. S. Uphade, Y. Yamada, T. Akita, T. Nakamura and M. Haruta, *Appl. Catal. A: Gen.* **215**, 137 (2001)
13. A. K. Sinha, S. Seelan, T. Akita, S. Tsubota and M. Haruta, *Catal. Lett.* **85**, 223 (2003)
14. G. C. Bond and D. T. Thompson, *Catal. Rev.-Sci. Eng.* **41**, 319 (1999)
15. A. Wolf and F. Schuth, *Appl. Catal. A: Gen.* **226**, 1 (2002)
16. L. G. Olson, Y. S. Lo, T. P. Jr. Beebe and J. M. Harris, *Anal. Chem.*, **73**, 4268 (2001)
17. B. Neiman, E. Grushka and O. Lev, *Anal. Chem.*, **73**, 5220, (2001)

18. G. Schmid, *Chem. Rev.* **92**, 1709 (1992)
19. R. P. Andreas, J. D. Bielefeld, J. I. Henderson, D. B. Janes, V. R. Kolagunta, C. P. Kubiak, W. J. Mahoney and R. G. Osifchin, *Science* **273**, 1690 (1996)
20. A. Kusumi, Y. Sako and M. Yamamoto, *Biophys. J.*, **65**, 2021, (1993)
21. J. W. Slot and H. J. Geuze, *J. Cell. Biol.*, **90**, 533, (1981)
22. P. Mulvaney, *MRS Bull.*, **26**, 1009, (2001)
23. F. Meriaudeau, T. Downey, A. Wig, A. Passian, M. Buncick and T. L. Farrell, *Sens. Actuators*, **B54**, 106, (1999)
24. Y. Jin, X. Kang, Y. Song, B. Zhang, G. Chang and S. Dong, *Anal. Chem.*, **73**, 2843 (2001)
25. I. Tanahashi, Y. Manabe, T. Tohda, S. Sasaki and A. Nakamura, *J. Appl. Phys.*, **79**, 1244 (1996)
26. M. Valden, S. Pak, X. Lai and D. W. Goodman, *Catal. Lett.* **56**, 7 (1998)
27. Y. Yuan, A. P. Kozlova, K. Aksura, H. Wan, K. Tsai and Y. Iwasawa, *J. Catal.* **170**, 191 (1997)
28. R. J. H. Griesel, P. J. Kooyman and B. E. Nieuwenhuys, *J. Catal.* **191**, 430 (2000)
29. G. R. Bamwenda, S. Tsubota, T. Nakamura and M. Haruta, *Catal. Lett.* **44**, 83 (1997)
30. J.-D. Grunwaldt, C. Kiener, C. Wogerbauer and A. Baiker, *J. Catal.* **181**, 223 (1999)
31. J.-D. Grunwaldt, M. Maciejewski, O. S. Becker, P. Fabrizioli and A. Baiker, *J. Catal.* **186**, 458 (1999)

32. M. M. Schubert, S. Hackenberg, A. C. van Veen, M. Muhler, V. Plzak and R. J. Behm, *J. Catal.* **197**, 113 (2001)
33. S. D. Lin, M. Bollinger and M. A. Vannice, *Catal. Lett.* **17**, 245 (1993)
34. S. K. Tanielyan and R. L. Augustine, *Appl. Catal. A: Gen.* **85**, 73 (1992)
35. A. I. Kozlov, A. P. Kozlova, K. Asakura, Y. Matsui, T. Kogure, T. Shido and Y. Iwasawa, *J. Catal.* **196**, 56 (2000)
36. T. V. Chaudhary, C. Sivadinarayana, C. Chusuei, A. K. Datye, J. P. Fackler Jr., and D. W. Goodman, *J. Catal.* **207**, 247 (2002)
37. Ph. Buffat and J.-P. Borel, *Phys. Rev. A* **13**, 2287 (1976)
38. M. Haruta, *Catal. Today* **36**, 153 (1997)
39. S. Tsubota, D.A. H. Cunningham, Y. Bando and M. Haruta, *Stud. Surf. Sci. Catal.* **91**, 227 (1995)
40. M. Valden, X. Lai and D. W. Goodman, *Science* **281**, 1647 (1998)
41. M. Okumura, S.-I. Nakamura, S. Tsubota, T. Nakamura and M. Haruta, *Stud. Surf. Sci. Catal.* **118**, 277 (1998)
42. T. V. Chaudhary and D. W. Goodman, *Topics in Catalysis* **21**, 25 (2002)
43. A. Kozlov, A. P. Kozlova, H. Liu and Y. Iwasawa, *Appl. Catal. A: Gen.* **182**, 9 (1999)
44. A. Cassell, J. Raymakers, J. Kong and H. Dai, *J. Phys. Chem. B* **103**, 6484 (1999)
45. H. Dai, J. Kong, C. Zhou, N. Franklin, T. Tomblor, A. Cassell, S. Fan and M. Chapline, *J. Phys. Chem. B* **103**, 11246 (1999)
46. P. A. Sermon and J. Sivalingam, *Colloids Surf.* **63**, 59 (1992)
47. R. J. H. Griesel and B. E. Nieuwenhuys, *J. Catal.* **199**(1), 48 (2001)

48. M. Okumura, S. Nakamura, et al, *Catal. Lett.* **51**, 53 (1998)
49. C. M. Yang, *Chem. Mater.* **15**, 275 (2003)
50. F. E. Wagner, S. Galvagno, C. Milone, A. M. Visco, L. Stievano and S. Calogero, *J. Chem. Soc. Faraday Trans.* **93**(18), 3403 (1997)
51. S. Qiu, R. Ohnishi and M. Ichikawa, *J. Phys. Chem.* **101**, 2719 (1994)
52. T. M. Salama, T. Shido, H. Minagawa and M. Ichikawa, *J. Catal.* **152**, 322 (1995)
53. T. M. Salama, R. Ohnishi and M. Ichikawa, *J. Chem. Soc., Faraday Trans.* **92**, 301 (1996)
54. D. Guillemot, M. Ploisset-Thfoin and J. Fraissard, *Catal. Lett.* **41**, 143 (1996)
55. V. Y. Borovkov, V. B. Kazansky, M. Ploisset-Thfoin and J. Fraissard, *J. Chem. Soc., Faraday Trans.* **93** (1997)
56. Y. M. Kang and B.-Z. Wan, *Appl. Catal. A: General* **128**, 53 (1995)
57. Y. M. Kang and B.-Z. Wan, *Catal. Today* **26**, 59 (1995)
58. Y. M. Kang and B.-Z. Wan, *Catal. Today* **35**, 379 (1997)
59. T. M. Salama, T. Shido, R. Ohnishi and M. Ichikawa, *J. Phys. Chem.* **100**, 3688 (1996)
60. D. Horvat, M. Polisset-Thfoin, J. Fraissard and L. Guzzi, *Solid State Ionics*, **141-142**, 153 (2001)
61. Z.-X. Gao, Q. Sun, H.-Y. Chen, X. Wang and W. M. H. Sachtler, *Catal. Lett.* **72**, 1 (2001)
62. K. Kuge and G. Calzaferri, *Micropor. Mesopor. Mater.* **66**, 15 (2003)
63. I. Mekkawy and M. M. Mohamed, *Egypt. J. Sol.* **25**(1), 115 (2002)

64. M. M. Mohamed, T. M. Salama and M. Ichikawa, *J. Colloid and Interface Sci.* **224**, 366 (2000)
65. R. Zhao, D. Ji, G. Lv, G. Qian, L. Yan, X. Wang and J. Suo, *Chem. Commun.* 904 (2004)
66. A. Gosh, C. R. Patra, P. Mukherjee, M. Sastry and R. Kumar, *Micropor. Mesopor. Mater.* **58**, 201 (2003)
67. J.-H. Liu, Y.-S. Chi, H.-P. Lin, C.-Y. Mou and B.-Z. Wan, *Catal. Today* **93-95**, 141 (2004)
68. K.-J. Chao, M.-H. Cheng, Y.-F. Ho and P.-H. Liu, *Catal. Today* **97**, 49 (2004)
69. B. S. Uphade, T. Akita, T. Nakamura and M. Haruta, *J. Catal.* **209**, 331 (2002)
70. B. S. Uphade, M. Okumura, S. Tsubota and M. Haruta, *Appl. Catal. A: General* **190**, 43 (2000)
71. Z. Konya, V. F. Puentes, I. Kiricsi, J. Zhu, J. W. Ager, et al, *Chem. Mater.* **15**, 1242 (2003)
72. P. Mukherjee, M. Sastry and R. Kumar, *Phys. Chem. Commun.* 4 (2000)
73. Y. Guari, C. Thieuleux, A. Mehdi, C. Reye, R. J. P. Corriu, S. Gomez-Gallardo, et al, *Chem. Commun.* 1374 (2001)
74. H. G. Zhu, B. Lee, S. Dai and S. H. Overbury, *Langmuir* **19**, 3974 (2003)
75. C. M. Yang, M. Kalwei, F. Schuth and K. J. Chao, *Appl. Catal. A:* **254**, 289 (2003)
76. P. Mukherjee, C. R. Patra, R. Kumar and M. Sastry, *Phys. Chem. Commun.* 5 (2001)
77. W. N. Delgass, M. Boudart and G. Parravano, *J. Phys. Chem.* **72**, 3563 (1968)

78. G. Steinbach and E. van der Lingen, *A novel Route for the Preparation of Supported Gold Catalysts for Low-Temperature CO Oxidation*, "Gold 2003: New Industrial Applications for Gold", Vancouver, Canada, 28 September to 01 October 2003.
79. S. Nagamatsu, M. Ichikuni, S. Shimazu, T. Fujikawa, K. Fukuda and T. Uematsu, *Au L₃-edge XANES Analyses for spr-Au/Al₂O₃ Catalyst*, "Gold 2003: New Industrial Applications for Gold", Vancouver, Canada, 28 September to 01 October 2003.
80. T. Uematsu, L. Fan, T. Maruyama, N. Ichikuni and S. Shimazu, *J. Mol. Catal. A: Chem.* **182-183**, 209 (2002)
81. C. Sivadinarayana, D. Kumar, Z. Yan, J. H. Lunsford and D. W. Goodman, *Catalytic Studies on Supported Nano-gold Catalysts*, Gold 2003: New Industrial Applications for Gold", Vancouver, Canada, 28 September to 01 October 2003.
82. C.-H. Lin, S.-H. Hsu, M.-Y. Lee and S. D. Lin, *J. Catal.* **209**(1), 62 (2002)
83. J. Lin, W. Zhou, A. Kumbhar, J. Wiemann, J. Fang, E. E. Carpenter and C. J. O'Connor, *J. Solid State Chem.* **159**, 26 (2001)
84. M. Toprak, D. K. Kim, M. Mikhailova and M. Muhammed, *Mater. Res. Soc. Symp. Proc.* **705**, Y7.22.1 (2002)
85. C. Li, D. Zhang, S. Han, X. Liu, T. Tang and C. Zhou, *Adv. Mater.* **15**(2), 143 (2003)
86. J. M. Kim and R. Ryoo, *Bull. Korean Chem. Soc.* **17**, 66 (1996)
87. M. Brust, M. Walker, D. Bethell, D. J. Schiffrin and R. Whyman, *J. Chem. Soc., Chem. Commun.* 801 (1994)

88. M. Brust, J. Fink, D. Bethell, D. J. Schiffrin and C. Kiely, *J. Chem. Soc., Chem. Commun.* 1655 (1995)

89. <http://www.montgomerychemical.com/Products/BoroMet1240.pdf>

90. L. Y. Chen, S. Jaenicke and G. K. Chuah, *Micropor. Mater.* **12**, 323 (1997)

91. N.-Y. He, S. L. Bao and Q. H. Xu, *Stud. Surf. Sci. Catal.* **105**, 85 (1997)

92. N.-Y. He, Z. Lu, C. Yuan, J. Hong, C. Yang, S. Bao and Q. Xu, *Supramol. Sci.* **5**, 553 (1998)

93. J. Turkevich, P. C. Stevenson and J. Hillier, *Discuss. Faraday Soc.* (11), 55 (1951)

94. G. Frens, *Nature Phys. Sci.* **241**, 20 (1973)

95. D. A. Handley, In *Colloidal Gold-Principles, Methods, and Applications*, M. A. Hayat, Ed., Academic Press, New York, vol. 1, p. 13, (1989)